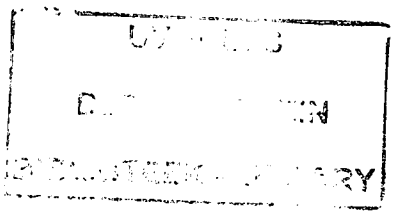

BIOLOGICAL SYNTHESIS OF GOLD NANOPARTICLES BY YEASTS

BY

SANDILE LAWRENCE FUKU

Submitted in fulfilment of the requirements
for the degree

MAGISTER SCIENTIAE

in the

Faculty of Natural and Agricultural Sciences
University of the Free State,
Department of Microbial, Biochemical and Food Biotechnology,
P.O Box 339,
Bloemfontein 9300
Republic of South Africa

September 2008

Supervisor : Prof. Esta van Heerden
Co-supervisor : Dr. Lizelle Piater

Table of contents

Acknowledgements

Thanks to Prof. Esta van Heerden for the invaluable support and assistance. I may have not inherited everything I need for survival but the environment you created around me gave me everything. I am greatly indebted to you.

Dr. L. Piater your willingness to help at all times is appreciated.

To Prof. D. Litthauer, I still remember the reassuring words you had for me in 2003. If it was not for you, I don't know were I could have been.

Prof. P. van Wyk and Jacqui, I appreciate your assistance and generosity in preparing TEM samples.

The Extreme biochemistry/Molecular group, your guidance and patience is greatly appreciated; I learnt a lot from you guys. One of the former Extreme biochemistry group members I ought to thank is Dr. Raji for being a good friend in and outside the lab.

I should appreciate and thank my family " Ndiyabulela Mapondomise" for the unconditional love and support. O.C Msimanga I value your companionship.

To the comrades I met in the department – thank you for the brotherhood and sisterhood.

To God and my ancestors- let light prevail on darkness.

Special thanks to: NRF for the financial support

"The principle of physics, as far as I can see, does not speak against the possibility of manoeuvering things atom by atom. It is not an attempt to violate any laws, it is something, in principle, that can be done, but in practice, it has not been done because we are too big."

Feynman, 1959

List of Abbreviations

BCA	Bicinchoninic acid
BIM	Biologically induced mineralization
BOB	Boundary organised biomineralization
bp	Base pair(s)
BSA	Bovine serum albumin
CAPS	*N*-cyclohexyl-3-aminopropanesulfonic acid
CNTs	Carbon nanotubes
DER736	Diglycidyl ether of polypropylene glycol
DNA	Deoxyribonucleic acid
DMAE	(S1) dimethylaminoethanol
EDTA	Ethylenediaminetetraacetic acid
EDS	Energy dispersive X-ray spectroscopy
EPS	Extracellular polysaccharides
$FADH_2$	Flavin adenine dinucleotide
HEPES	N-(2-hydroxyethyl)-piperazine-N'-2-ethanesulfonic acid
H	Hour
kDa	kilo Dalton
LSPR	Localized surface plasmon resonance
LSU	Large sub-unit
MWNTs	multi wall carbon nanotubes
NADH	Nicotinamide adenosine dinucleotide
NADPH	Nicotinamide adenosine dinucleotide phosphate
NTA	Nitriloacetic acid
O.D	Optical density
ODA	Octadecylamine
pI	Iso-electric point
PVP	Polyvinylpyrrolidone
PCR	Polymerase chain reaction

QDs	Quantum dots
QC	Quasi crystal
rpms	Revolutions per minute
SAMs	Self assembly monolayers
SDS PAGE	Sodium dodecyl sulfate polyacrylamide gel electrophoresis
StA	Stearic acid
SWNTs	Single wall carbon nanotubes
TEM	Transmission electron microscopy
UHV	Ultrahigh vacuum
UFS	University of the Free-State
UV-Vis	Ultra violet and Visible
VCD	Vinylcyclohexene dioxide

List of Figures

Figure 1.6: Simple model for biogeochemical significance of metal and metalloid transformations by fungi. Their influence in effecting changes in metal solubility is emphasized, as well as the influence of environmental factors on these processes and on fungal growth, morphogenesis and physiology. The relative balance between the processes will depend on the environment, organism(s), and interactions with other organisms including animals, plants and anthropogenic activities. (1), Metal solubilization by, e.g., heterotrophic leaching, siderophores, metabolite excretion including organic acids and H^+, redox reactions, methylation, and biodegradation of organometal(loid)s. (2), Effect of soluble metal species on fungi and metal immobilization by e.g. biosorption, transport, intracellular sequestration and compartmentation, redox reactions, precipitation, and crystallization. (3), Effect of insoluble metal species on fungi, particulate adsorption, and entrapment by polysaccharide and/ or mycelial network. (4), Metal immobilization by, e.g. precipitation, crystallization, or reduction. (5), Influence of environmental factors, e.g., pH, O_2 , CO_2, nutrients, salinity, toxic metals, pollutants on fungal growth, metabolism, and morphogenesis. O_2, CO_2, and redox potential, depletion of nutrients, enzyme and metabolite excretion. (7) and (8), Environmental factors which direct the equilibrium between soluble and insoluble metal species towards metal mobilization (7) or metal immobilization (8) (Taken from Gadd,1996; Morley *et al.,* 1996; White *et al.,*1997)

(15)

Figure 1.7: TEM micrographs of *F. oxysporum* synthesized nanoparticles immobilized in a 500 angstrong() thick StA film at pH 4.5 (A) and in a 500 amstrong thick ODA film at pH 6.6. (Taken from Shankar *et al.,* 2004).

(18)

List of Tables

Chapter 1
Literature review

1.1. General introduction

Nanotechnology is defined as the technology development at the atomic or molecular range of approximately 1-100 nanometers (nm) to create and use structures, devices and systems that have novel properties (Whitesides, 2003). The name "nano" comes from the size of molecule which is measured in nanometers or one billionth of a meter (10^{-9} m). As far as the synthesis of nanoparticles is concerned, a number of chemical methods exist in literature that use toxic chemicals in the synthesis protocol, which raises great concern for environmental reasons (Mukherjee *et al.*, 2001). This necessitates "NANOBIOTECHNOLOGY".

Nanobiotechnology is defined as the application of nanoscaled tools to biological systems or the use of the biological systems as templates in the development of novel nanoscaled products (Fortina *et al.*, 2005). Nanoparticles of metals such as gold, silver, platinum, lead, palladium and cadmium have been synthesized by material scientists. The unusual physicochemical and optoelectronic properties of nanoparticles arise primarily due to confinement of electrons within particles of dimensions smaller than the bulk electron delocalization length; this process is termed quantum confinement (Shi *et al.*, 1996).

Metal nanoparticles of varying sizes can be prepared by many physical and chemical methods with some degree of control. The primary disadvantage of these techniques are high operating temperatures and pressures, use of organic solvents (harsh, expensive chemicals), potential lack of scalability, and still limited control over crystalline size dispersion (Zang *et al.*, 2007). There is a need to develop clean, non-toxic and environmentally friendly synthetic procedures for nanoparticles (Mukherjee *et al.*, 2001). In this regard, biological

systems are well suited for nanoparticle synthesis as most of cell machinery is at a nanoscale e.g. ribosomes involved in protein synthesis. Most importantly metal tolerance in microorganisms is well documented with at least one mechanism being reduction of metal ions to their respective elemental states (Nies, 1999).

Two fundamentally different modes of biomineralization are summarized by Lowenstam and Weiner (1989). One is biologically induced mineralization (BIM), in which an organism modifies its local microenvironment creating conditions suitable for chemical precipitation of extracellular mineral phases. The second mode is called boundary organized biomineralization (BOB), in which inorganic particles are grown within or on some organic matrix produced by the organism (Mann *et al.*, 1990a).

Bacteria that produce mineral phases by BIM do not strictly control the crystallization process, resulting in particles with no unique morphology and broad particle size distribution. For example, the iron reducing bacterium *Geobacter metallireducens* is a non-magnetotactic anaerobe that couples the oxidation of organic matter to the reduction of ferric iron, inducing the extracellular precipitation of fine grained magnetite as a by product (Lovely, 1990). In laboratory culture, *Geobacter metallireducens* can produce 5000 times more magnetite by weight than an equivalent biomass of magnetotactic bacteria. However, magnetic measurements show that most of the *Geobacter metallireducens* produced particles are magnetically unstable with size range (<20 nm) at room temperature.

Contrary to BIM, bacteria that produce mineral phase by a BOB process exert strict control over size, morphology, composition, position and crystallographic orientation of the particles (Mann *et al.*, 1990b). These bacteria synthesize intracellular, membrane bounded Fe_3O_4, Fe_3S_4 and FS_2 particles called magnetosomes. Various arrangements of magnetosomes within cells impart a

permanent magnetic dipole moment to the cell, which effectively makes each cell a self propelled biomagnetic compass.

One of the most challenging problems in chemical synthesis of nanoparticles has been the controlled synthesis of monodispersed size and morphology of these nanoparticles.

Biological systems have been found to produce specifically tailored nanostructures with highly optimized properties and characteristics. Different publications reported gold synthesis using *Thermospora* sp. (actinomycete), *Verticillium* sp. and *Fusarium oxysporum* (fungi). Klaus and his co-workers (1999), reported silver nanoparticles synthesized by *Pseudomonas stutzeri*. In 2002, Nair and Pradeep demonstrated gold nanoparticle synthesis using a *Lactobacillus* strain.

1.2. Chemical synthesis of metal nanoparticles

There is no agreed definition of a nanoparticle but they are commonly considered to be particles having a dimension less than 100 nm (Antken *et al.*, 2004). The development and application of nanoparticles represent a major portion of nanotechnology activity and the number of nanoparticle products continues to grow. Many different techniques have been developed to generate metal nanoparticles. There are two general strategies to obtain materials on the nanoscale.

The first method is called top down method, where material is removed from the bulk material, leaving only the desired nanostructures. Typical top down techniques are photolithography and electron beam lithography (Liu *et al.*, 2000).

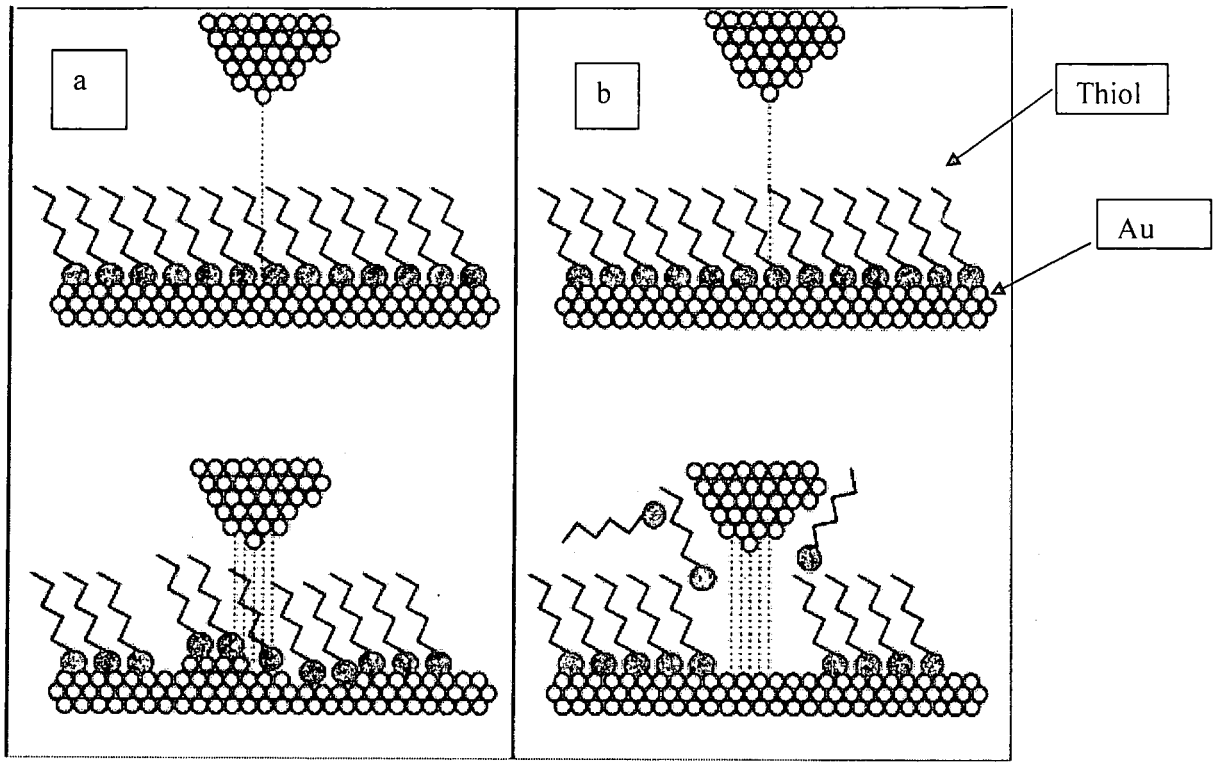

Figure 1.1: Schematic diagrams depicting two basic manipulations, electron induction diffusion (a) and electron induced evaporation (b) mechanisms in lithography. The imaging and fabrication modes are depicted in top and bottom rows, respectively (Adapted from Liu *et al.*, 2000).

Tunnelling electrons are used to achieve nanoparticle formation in lithography as illustrated in Figure 1.1. Self Assembly Monolayers (SAMs) are first imaged under a very low tunnelling current. Under ultrahigh vacuum (UHV), the tunneling is slowly increased while the bias voltage is maintained constant. As the tunnelling current is increased beyond a certain threshold, displacement of metal atoms or desorption of adsorbate molecules occurs (bottom panels in Figure 1.0 (a) and (b)). The newly exposed gold is spatially confined by surrounding thiols (Liu *et al.*, 2000). Top down techniques require removal of large amounts of material, thus less favourable.

Second, bottom up approach whereby atoms are generated from the reduction of their respective ions, atoms are then assembled into nanostructures (Haes *et al.*, 2004b).

The bottom up method has the disadvantage of producing polydispersed particles, due to the need to arrest growth at the same time for all particles. Bottom up techniques include nanosphere lithography. These methods require a closely packed monodisperse layer of polystyrene spheres having sizes that are hundreds of micrometers in diameter. The spheres are deposited on a substrate that acts as a template for metal deposition. The metal of interest is then deposited onto and in between the spheres using thermal evaporation to create particles in the voids of the polystyrene spheres. The polystyrene spheres are dissolved in an organic solvent leaving triangular nanoparticles as observed in Figure 1.2.

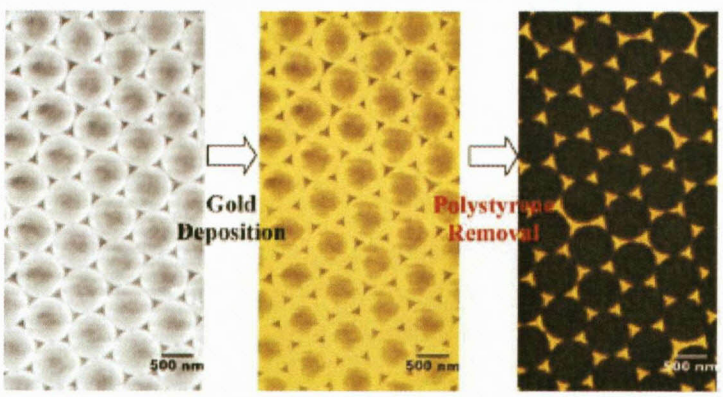

Figure 1.2: Deposition of polystyrene spheres on substrate, thermal evaporation of bulk gold and removal of polystyrene spheres to leave triangular gold nanoparticles (Huang *et al.*, 2005).

Other bottom up techniques usually employs an agent to arrest growth of the particles at nanoscale. Capping materials, such as surfactants or polymers are used in these techniques to prevent aggregation and precipitation of metal nanoparticles out of solution. Choice of the reduction technique, time, and capping material determines the size and shape of the formed nanoparticles (Haes *et al.*, 2004b).

The purpose of producing these new materials and products is that their behaviour is expected (and has been demonstrated) to be different in nanometer scale than in macroscale (Antken *et al.,* 2004). Table 1.1 shows that particle morphology is a useful basis of categorising nanoparticles.

Table 1.1 Nanoparticles - categories and application (Taken from Jorter and Rao, 2002.)

Nanostructures	**Example Material or Application**
Nanotubes	Carbon, (fullerens)
Nanowires	Metals, semiconductors, sulphides, nitrides
Nanocrystals, quantum dots	Insulators, semiconductors, metals, magnetic materials
Other nanoparticles	Ceramic oxides, metals

1.2.1 *Nanotubes*

Carbon nanotubes (CNTs) were first discovered by Iijima (1991) and are a new form of carbon molecule. They are elongated to form tubular structures 1-2 nm in diameter. They can be produced with a very large aspect ratio and can be 1 mm in length. In their simplest form, nanotubes comprise a single layer of carbon atoms (single molecules) arranged in a cylinder. These are known as single wall carbon nanotubes (SWNTs). They can also be formed as multiple concemetric tubes (multi wall carbon nanotubes, MWNTs) having a diameter significantly greater or equal to 10 nm, and length greater than 1 mm (Treacy *et al.,* 1996).

CNTs have great tensile strength and are considered to be 100 times stronger than steel whilst being one sixth of its weight thus making them potentially the strongest, smallest fiber known. They also exhibit high conductivity, high surface area, unique electronic properties, and potentially high molecular adsorption

capacity (Maynard *et al.,* 2004). Applications which are currently being investigated include polymer composites (conductive and structural filler), electromagnetic shielding, electron field emitters (flat panel displays), super capacitors, batteries, hydrogen and structural composites (Frank *et al.,* 1998).

1.2.2 *Nanowires*

Nanowires are small conducting or semi-conducting nanoparticles with a single crystal structure and a typical diameter of a few tens of nanometers and a larger aspect ratio. They are used as interconnectors for the transport of electrons in nanoelectronic devices. Various metals have been used to fabricate nanowires including cobalt, gold, and copper. Silicon nanowires have also been produced (Antken *et al.,* 2004).

1.2.3 *Quantum dots*

Quantum dots (QDs) of semiconductors, metals, and metal oxides are gaining recognition due to their novel electronic, optical, magnetic and catalytic properties. The number of atoms in a quantum dot, which range from 1000 to 100 000 makes it neither an extended solid structure nor a single molecular entity. This led to various names being attributed to such materials including nanocrystals and artificial atoms (Grieve *et al.*, 2000).

The majority of nanoscience research has centered around quantum dots as they exhibit distinct 'quantum size effects. The light emitted can be tuned to desired wavelengths by altering the particle size (Antken *et al.,* 2004). Multiplex tagging of unknown molecules (different DNA fragments or proteins) in a sample and their subsequent tag-by-tag recognition in a flow system provides an appealing alternative to monitoring a binding event and single colour detection 'by location' in planar, fixed arrays. Highly multiplex tags have been developed based on QDs (Antken *et al.*, 2004).

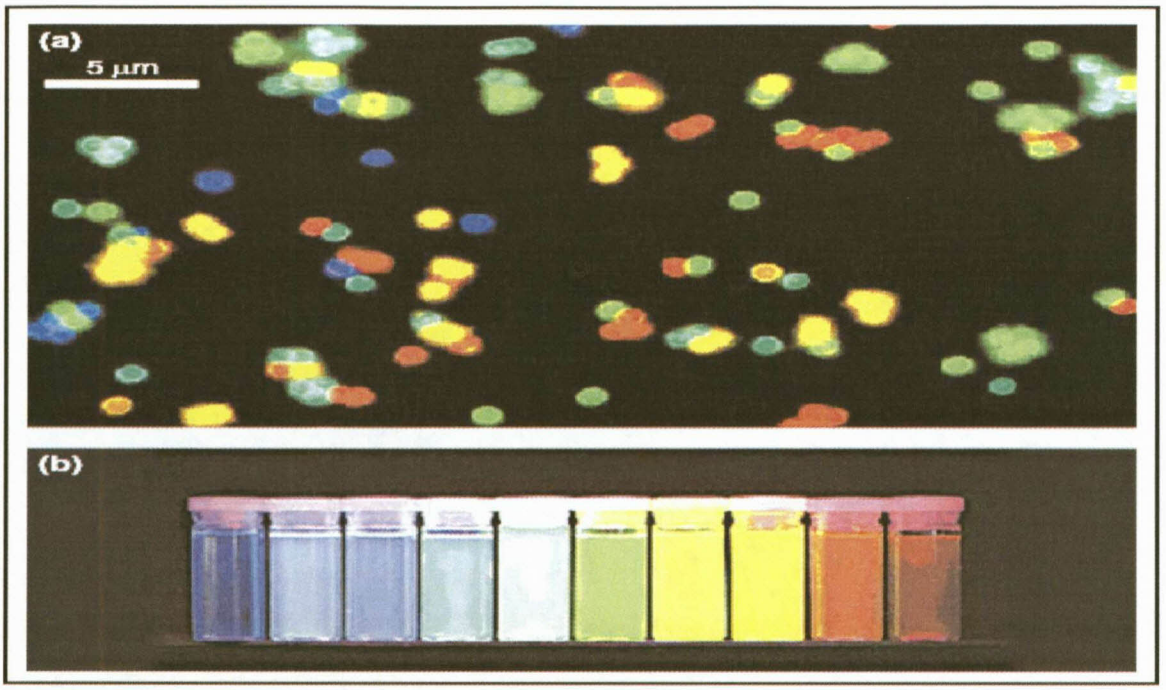

Figure 1.3: Quantum-dot-tagged microbeads for multiplexed optical coding of biomolecules. (a) Fluorescence micrograph of a mixture of CdSe/ZnS QD-tatagged beads emitting single-colour signals at 484, 508, 547, 575, and 611nm. The beads were spread and immobilized on polylysine-coated glass slide, which caused a slight clustering effect. (b) Ten distinguishable emission colours of ZnS-capped CdSe QDs excited with a near-uv lamp (Taken from Han *et al.*, 2001).

1.2.4 *Other nanoparticles*

This category includes a wide range of primarily spherical or aggregated dendritic forms of nanoparticles. Dendritic forms where spherical or other compact forms of primary particles aggregate together to form chain like or branching structures. Welding fume is the best known example of this. Nanoparticles of this type may be formed from many materials including metals, oxides, ceramics, semiconductors and organic material. The particles may be composites having, for example, a metal core with an oxide shell or alloys in which a mixture of metals are present (Jorter and Rao, 2002).

1.2.5 *Metal Nanoparticles*

Precious metal nanoparticles exhibit a strong UV-visible absorption band that is not present in the spectrum of bulk metal. This absorption band result when the incident photon frequency is resonant with the collective excitation of the conduction electrons and is known as the (LSPR) localized surface plasmon resonance (Haes *et al.*, 2004a).

1.2.5.1 *Gold*

Reduction of the gold chloride to gold metal is performed by UV irradiation either directly in solution or on cast films (Carrot *et al.*, 1998). UV irradiation has the advantage of not provoking reactions with the polymer, which a chemical reducing agent might do. The reader is reminded that many bacteria have the ability to selectively reduce metals, a property that will feature in the discussion of microorganisms and their role in synthesis of metal nanoparticles.

Nanoparticles synthesized chemically are of poor monodispersity. The chemical method relies upon the self-assembly properties of surfactant/polymer (micellar co-operative aggregates) which so form interactions with the metal or metal ions during ion reduction. The hydrophobic segments are directly adsorbed on the surface of the newly formed 'hydrophobic' solid nano-metal for its stabilisation and the hydrophilic segments spread out into the hydrophilic solvent (Carrot *et al.*, 2004). Dietrich *et al.* (2005) demonstrated that gold nanoparticles can be used for spectral imaging in proteomics. The property of different nanoparticles to scatter light at different wavelengths was exploited in generating spectra as seen in Figure 1.4.

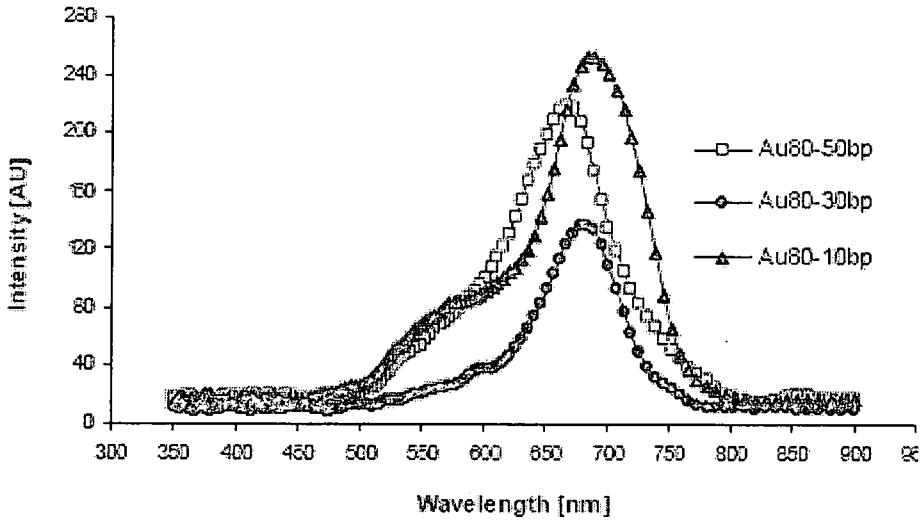

Figure 1.4: Spectra of different sized oligonucleotides measured with a SpectraCube®, □ 50 bp, ⧈ 30 bp and ▲ 10 bp sized oligonucleotides. The size of gold nanoparticles is 80 nm in diameter (Dietrich *et al.*, 2005).

1.2.5.2 *Silver*

Sun and Xia (2002) reported synthesis of silver nanocubes by reducing silver nitrate with ethylene glycol at 160 °C, in the presence of a capping reagent poly vinyl pyrrolidone (PVP). These cubes were single crystals and were characterized by a slightly truncated shape bounded by facets. The presence of PVP and its molar ratio (in terms of repeating unit) relative to silver nitrate both played important roles in determining the geometric shape and size of the product. The morphology and shape of these particles were also found to be dependent on temperature i.e. a temperature drop from 190 °C to 120 °C resulted in irregular shapes. These silver nanoparticles are envisaged to find application in a variety of areas that include photonics, catalysis and electronic based sensors (Sun and Xia, 2002).

1.2.5.3 *Platinum*

Platinum nanoparticles synthesis in non-polar organic solvents has been archived in a reaction involving extraction of platinum ions into toluene using a phase transfer molecule (tetra-alkyl ammonium bromide), followed by reduction of metal ions using sodium borohydride in the presence of capping agent (thiol/alkylamine). This resulted in platinum metal nanoparticles. The phase transfer was accomplished by vigorous shaking and octadecylamine in hexane. During shaking of the biphasic mixture, the aqueous platinum nanoparticles form a complex with octadecylamine (ODA) molecules present in the organic phase. This renders the nanoparticle hydrophobic. This means platinum produced in this method is not really a pure metal, even though it has been found to have a high catalytic activity (Kumar *et al.*, 2004).

1.2.5.4 *Cadmium Nanoparticles*

CdS nanoparticle colloids are synthesized by mixing $Cd(ClO_4)_2$ and Na_2S in solution. The method is relatively inexpensive. The colloidal route permits the production of relatively pure nanoparticles, and as the matrix is liquid, the separation is easy. The dynamics of the formation of nanoparticles in a colloidal form is based on dissociation of the species present in the mixture solution and parameters like dielectric constant of the solvent, temperature and the concentration of the solutions (Pal *et al.*, 200). The stability of the colloidal particles is influenced by chemical equilibrium. In the case of CdS, the chemical equilibrium is defined by the reaction:

$$(CdS)_{CRYSTAL} \longleftrightarrow (Cd^{++})_{aq} + (S^{--})_{aq}$$

The above equilibrium is a function of size of the crystallites and the dielectric constant of the solvent. The reaction is favoured to the right hand side due to the low energy of bonding in the small crystals and the dissolved ions can recrystallize to bigger particles (Pal *et al.*, 2000).

1.2.6 *Magnetic nanoparticles*

Organometallic complexes containing an olefinic or polyolefinic ligand act as precursors to be hydrogenated to give a bare metal atom which will be condensed in a reaction medium. Prototypes of such complexes are $Co(C_8H_{13})(C_8H_{12})$ and $Ni(C_8H_{12})_2$ which decompose satisfactorily under dihydrogen in mild conditions (Haes *et al.*, 2004a).

Thus, $Co(C_8H_{13})(C_8H_{12})$ decomposes readily at room temperature in solution in the presence of low pressure (generally 3 bar) of dihydrogen. When using PVP as a stabilizer, nanoparticles of 1.6 or 2 nm were obtained as a function of precursor concentration. The particles produced were super paramagnetic with blocking temperature near 10 k (-283°C) and display an enhanced magnetization at saturation per cobalt atom compared to bulk cobalt (Haes *et al.*, 2004a).

As in all naturally occurring crystals, the above-mentioned nanosphere masks include a variety of defects that arise as a result of nanosphere polydispersity, site randomness, point defects (vacancies), line defects (slip dislocations) and polycrystalline domains. Typical defect free domain sizes are in the 10 -100 μm range (Haes *et al.*, 2004a).

The first step in magnetite synthesis in magnetotactic bacteria is the uptake of iron. The magnetic nanoparticles are formed in the magnetosomes. In strains of *Magnetospirillum*, the magnetosome membrane was found to consist of a bilayer containing phospholipids and proteins, at least several of which appear unique to this membrane (Gorby *et al.*, 1988; Schüler and Baeuerlein, 1998). Although the protein patterns of the magnetosome membrane are distinguishable between different strains of *Magnetospirillum,* at least one major protein with a molecular weight of about 22 - 24 kDa appears to be common to all strains tested so far as revealed by sequence analysis and antibody cross-reactivity (Okuda *et al.*, 1996; Schuler and Baeuerlein, 1998). However, the exact role of the magnetosome-

specific proteins has not been elucidated and it has been speculated that they have a specific function in accumulation of iron, nucleation of minerals, redox and pH control (Gorby *et al.,* 1988; Mann *et al.,* 1990a). Figure 1.5 shows different morphologies of magnetosomes from different cells.

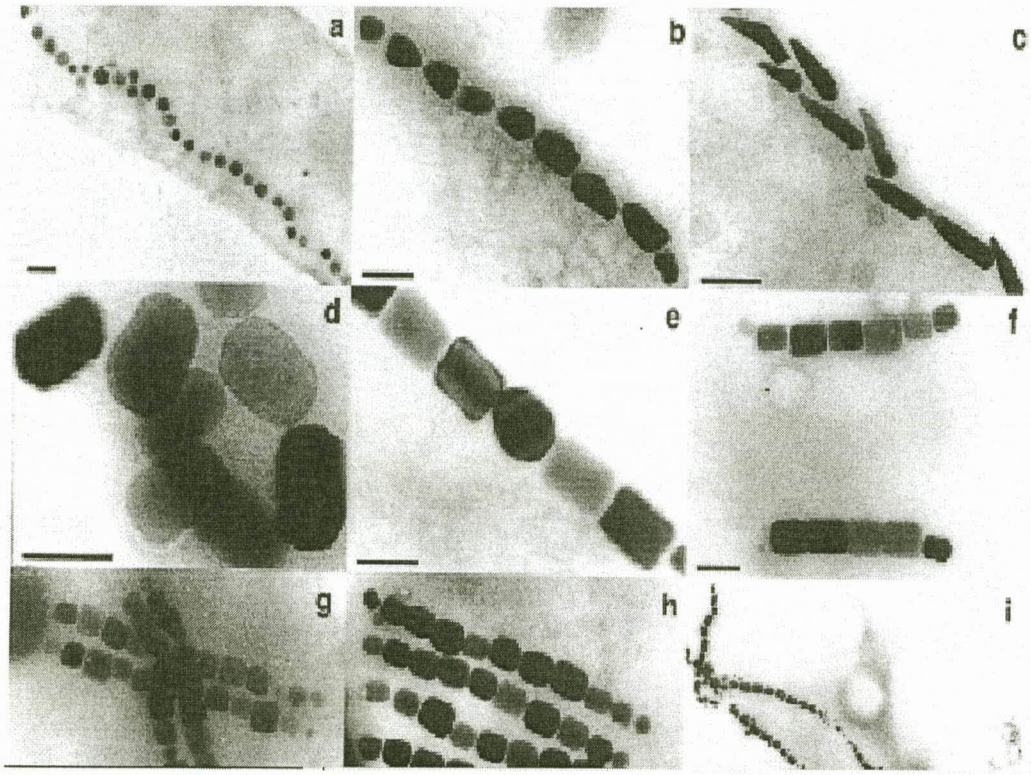

Figure 1.5: Morphologies of magnetosomes from different cells. Shapes of magnetic crystals include cubooctahedral (a), bullet shaped (b, c), elongated prismatic (d, e, f, g, h, i (Taken from Schüler, 1999).

1.3. Biological interactions with metals

Interaction between microorganisms and metals can be divided into three distinct processes namely intracellular, cell surface and extracellular interaction (Ford and Ryan, 1995).

1.3.1 *Intracellular interactions*

Assimilation of metal ions may be important to microorganisms in detoxification, enzyme function, and physical characteristics of the cell (Ford and Ryan, 1995). Several species of fungi, including unicellular and filamentous forms, can transform metals, metalloids, and organometallic compounds by reduction, methylation and dealkylation. These are processes of environmental importance since transformation of a metal or metalloid may modify its mobility and toxicity (Gadd, 1993).

The biological methylation of metalloids has been demonstrated in filamentous fungi and yeast, and frequently results in their volatilization (Gadd, 1993). Organometallic compounds can be degraded by fungi, either by direct biotic action (enzymes) or by facilitation of abiotic degradation, for instance by alteration of pH and excretion of metabolites (Gadd and Sayer, 2000).

1.3.2 *Cell-surface interaction*

Algal surfaces contain functional groups (e.g., carboxylic, amino, thio, hydroxo and hydroxyl-carboxylic groups) that can interact with metal ions (Xue *et al.,* 1988). Gram negative bacteria have lipopolysaccharides and phospholipids in their cell walls, with phosphoryl groups as the most abundant electronegative site available for metal binding (Coughlin *et al.,* 1983). Gram positive cell walls on the other hand possess teichoic acid and peptidoglycan, providing carboxyl and phosphorylgroups that are potential binding sites for metals (Doyle, 1989). For both gram positive and gram negative bacteria, metal binding to cell-surface functional groups is thought to be an essential step to intracellular accumulation of trace metals required for enzyme function. In addition, certain bacteria appear capable of using toxic metal species as electron acceptors, with both selenate and chromate reportedly reduced under anaerobic conditions (Oremland *et al.,* 1989).

1.3.3 *Extracellular interaction*

Many microorganisms produce extracellular polysaccharides (EPS), often containing proteins that strongly bind metals. Interaction between EPS and metal ions are generally considered a direct consequence of negatively charged functional groups on oxypolymers (Ford and Ryan, 1995).

Extracellular interaction with metals ranges from the potential to leach metals from sediments by production of acidic metabolites to the formation of colloidalised EPS-metal complexes implicated in mobilization and transport of toxic metals in soils (Black *et al.,* 1986; Chanmugathas and Bollag, 1988). EPS-metal interactions are of particular interest because of their ability to mobilize and transport metals. The ability to essentially bind toxic metals in the colloidal fraction of the organic carbon pool is important in the cycling of metals in any aquatic system (Ford and Ryan, 1995). Figure 1.6 summarises the above-mentioned interactions.

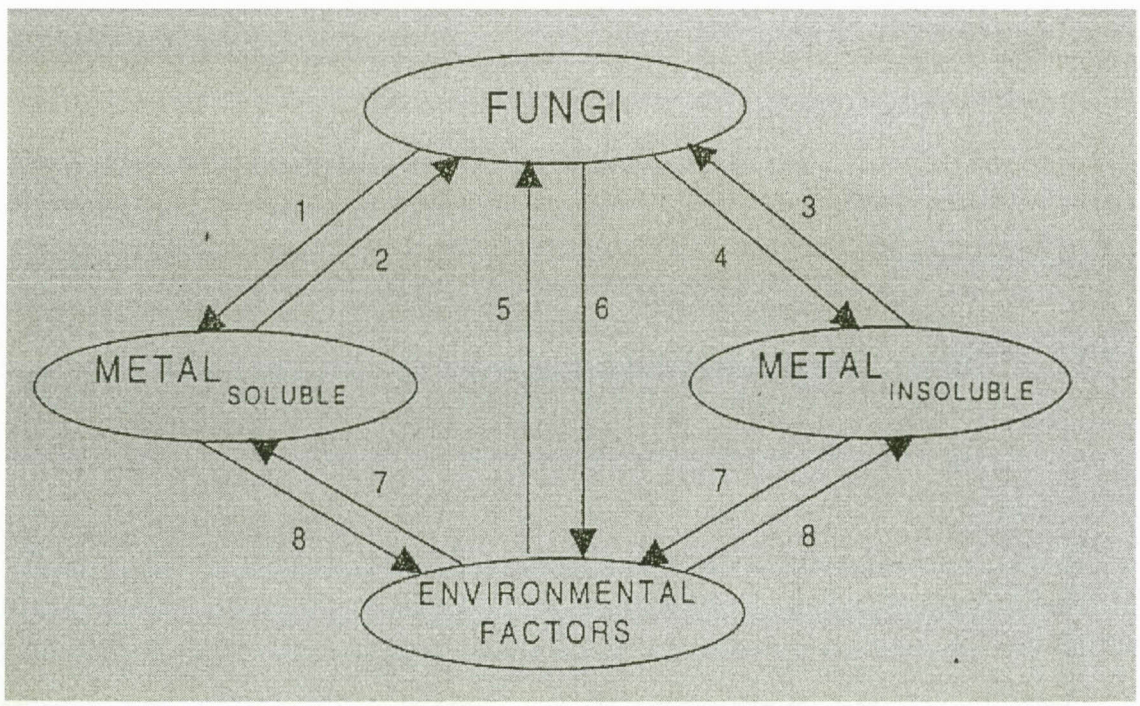

Figure 1.6: Simple model for biogeochemical significance of metal and metalloid transformations by fungi. Their influence in effecting changes in metal solubility is emphasized, as well as the

influence of environmental factors on these processes and on fungal growth, morphogenesis and physiology. The relative balance between the processes will depend on the environment, organism(s), and interactions with other organisms including animals, plants and anthropogenic activities. (1), Metal solubilization by, e.g., heterotrophic leaching, siderophores, metabolite excretion including organic acids and H^+, redox reactions, methylation, and biodegradation of organometal(loid)s. (2), Effect of soluble metal species on fungi and metal immobilization by e.g. biosorption, transport, intracellular sequestration and compartmentation, redox reactions, precipitation, and crystallization. (3), Effect of insoluble metal species on fungi, particulate adsorption, and entrapment by polysaccharide and/ or mycelial network. (4), Metal immobilization by, e.g. precipitation, crystallization, or reduction. (5), Influence of environmental factors, e.g., pH, O_2, CO_2, nutrients, salinity, toxic metals, pollutants on fungal growth, metabolism, and morphogenesis. O_2, CO_2, and redox potential, depletion of nutrients, enzyme and metabolite excretion. (7) and (8), Environmental factors which direct the equilibrium between soluble and insoluble metal species towards metal mobilization (7) or metal immobilization (8) (Taken from Gadd,1996; Morley *et al.,* 1996; White *et al.,*1997)

1.4 Microorganisms and their role in synthesis of metal nanoparticles

Many microorganisms are known to produce metals at a nanoscale with properties similar to those of chemically synthesized particles. This biosynthesis of metal nanoparticles requires that the organism be exposed to an environment that has metal ions of the metal of interest. Fungal, yeast and bacterial species have been reported to synthesize metal nanoparticles, either extracellularly or intracellularly.

Exposure of *Verticillium* sp. *(*AAAT-TS-4*)* to an aqueous solution of $HAuCl_4$ resulted in the formation of gold metal particles that were measured to be approximately 20 nm in diameter (Mukherjee *et al.,* 2001). Most of the gold particles were found on the cytoplasmic membrane rather than on the cell wall. The gold particles in this fungus were mostly of spherical, pseudo-triangular and hexagonal octahedral shaped and the dimensions were fairly monodispersed. Intracellular synthesis of gold nanoparticles was observed in the alkalotolerant actinomycete, *Rhodoccocus* sp. and most of gold nanoparticles were found on the cytoplasmic membrane than on cell wall (Ahmand *et al.,* 2003b). The size of the metal gold particles was about 12 nm and spherical in shape. Contrary to *Verticillium* sp. there was better monodispersity (Ahmand *et al.,* 2003b). This suggests that there is size and morphology regulation within *Verticillium* sp.

Extracellular synthesis of silver nanoparticle was achieved by growing *Fusarium oxysporum* in $AgNO_3$ containing solution (Ahmad *et al.,* 2003a). The silver particles produced were 5 to 15 nm in diameter. It is known that extracellular synthesis has some advantages over intracellular synthesis on practical considerations. When Ag^0 is recovered from the solution it can be conveniently immobilized on a stationary phase. Figure 1.7 shows size distribution of silver nanoparticles formed by *F. oxysporum* when nanoparticles are immobilized on films at different pH values.

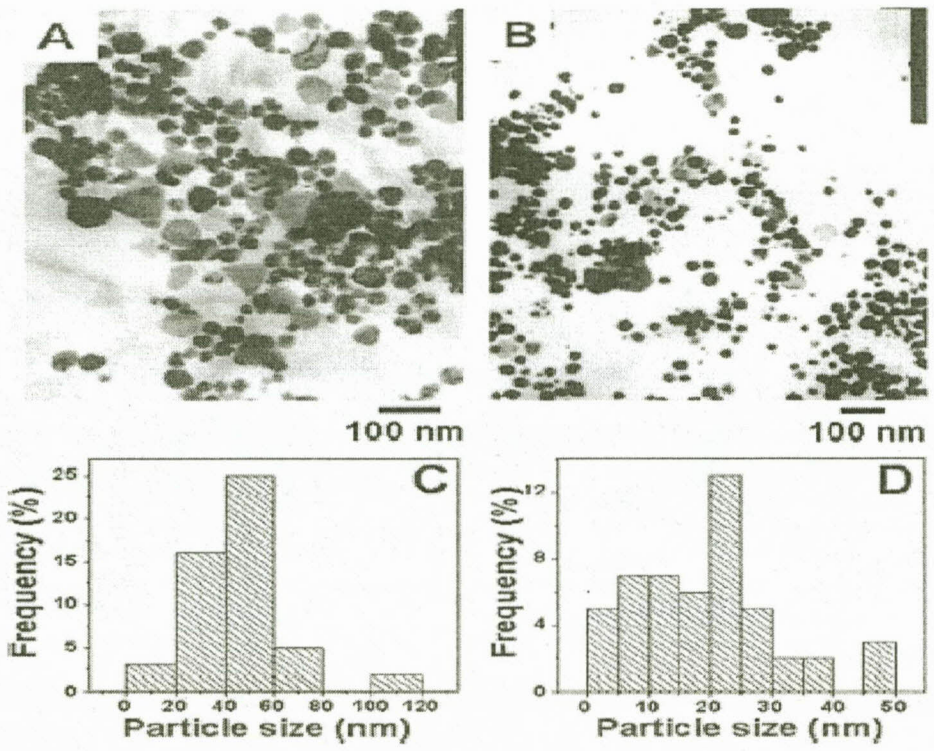

Figure 1.7: TEM micrographs of *F. oxysporum* synthesized nanoparticles immobilized in a 500 angstrom (Å) thick StA film at pH 4.5 (A) and in a 500 amstrong thick ODA film at pH 6.6(B). (Taken from Shankar *et al.,* 2004).

It was observed that when *Schizosaccharomyces pombe* in early exponential phase was subjected to 1 mM cadmium solution, $Cd_{16}S_{20}$ particles with 2 - 2.5 nm diameter and hexagonal shape formed. Under pressure of 20 - 40 kbars these nanoparticles converted into rock salt structure. This was similar to the properties of chemically synthesized particles (Kowshik *et al.,* 2001). Interesting to observe was that upon exposure to cadmium, the yeast activated phytochelatin synthase which synthesized phytochelatins having the basic structure (Glu-Cys)-Gly. Phytochelatins chelate the cytoplasmic cadmium to form a low molecular weight phytochelatin-Cd complex. Further, an ATP binding cassette (ABC) type vacuole membrane protein HMT-1, transports phytochelatin-Cd complex across the vacuole membrane. Within the vacuole, sulfide is added to the complex to form a high molecular weight phytochelatin-CdS^{-2} complex or the CdS nanocrystal (Ortiz *et al.,* 1995). The nanoparticles' size was

reproducible, more monodisperse and had a greater stability than synthetic nanoparticles.

Pseudomonas stutzeri AG259 was grown in 50 mM $AgNO_3$ solution (Klause *et al.,* 1999). Ag^0 crystals with well-defined composition and shape were observed. The nanoparticles produced were approximately 200 nm in size and had equilateral triangular and hexagonal shape. They were located on cell poles on the cytoplasmic membrane (Klaus *et al.,* 1999). Other studies reported silver nanoparticles from the same *P. stutzeri* to be in the range of 35 to 46 nm (Slawson *et al.,* 1992). This variability could be attributed to the difference in the cell growth and metal incubation conditions.

P. dimuta which was isolated from a mining environment was also found to produce Ag^0 nanoparticles. Two protein molecules might be associated with the silver binding properties of this bacterium in presence of silver (Ibrahim *et al.,* 2001). The result of this experiment showed the presence of low and high molecular weight proteins. Proteins bindind Ag^0 on the cytoplasmic membrane were of high molecular weight ($20 \times 10^3 - 14 \times 10^3$) and pI= 8 – 8.9. Proteins binding Ag^0 on cell wall were of low molecular weight ($10 \times 10^3 - 12.5 \times 10^3$) and pI= 1.7 – 2.0. It has also been reported that Fe^{+3} reducing microorganisms, that can reduce Au^{+3} have a specific mechanism for Au^{+3} reduction that is distinct from the mechanism for Fe^{+3} reduction (Kashefi *et al.,* 2001).

Pseudomonas aeruginosa PA01, a gram negative bacteria, produces two chemically distinct types of lipopolysaccharides, termed A-band and B-band LPS (Langley and Beveridge, 1999). The A-band O-side chain is electroneutral at physiological pH, while the B-band O-side contains negatively charged sides due to the presence of uronic acid residues in the repeat unit structure. Strain PAO1(A^+B^+) and three isogenic LPS mutants (A^+B^+, A^-B^+ and A^-B^-) were studied to determine the contribution of the O-side chain portion of LPS to metal binding by the surfaces of gram negative cells. When all these cells were exposed to

$AuCl_3$ and $Cu(NO_3)_2$ solutions respectively, it was observed that they bind similar amounts of copper (0.213 – 0.22 umol/mg dry weight of cell) and that in gold solution, they all resulted in intracellular formation of gold elemental crystals with few crystals bound to the cell surface (Langley and Beveridge, 1999).

This suggest that in this bacteria gold binding is not a surface mediated event and that negatively charged sites located in the O-side chain are not directly responsible for binding of metallic ions. It has been suggested that microorganisms may be involved in the formation of gold deposits when soluble Au^{+3} enters an environment in which microorganisms either alter environmental conditions to promote the precipitation of gold or adsorb Au^{+3} and then reduce it *via* unspecified reactions (Gadd and Sayer, 2000).

Shankar *et al. (*2003) reported the synthesis of gold from a mixture of geranium leaf extract and gold ions. However, the particles were polydispersed. This supports the thought of considering organic molecules to be central in nanoparticle formation. However, mechanisms by which nanoparticles form in biological systems and their extracts are still unknown.

Microoganisms can also affect metal speciation in different ways. Some processes involve redox reactions that occur during chemolithotrophic energy generations, as energy source metals can satisfy the energy demand of an organism (Erlich, 1997). For example, *Thiobacillus ferrooxidans* can obtain energy for growth from the reduction of Fe^{3+} to Fe^{2+} (Ingledew,1982). Others result from utilization of metals as electron acceptors and such reactions include the reduction of MnO_2 to $MnCO_3$ with acetate by *Eubacterium metallireducens* (Lovley and Phillips,1988). Transfer of electrons to the metal ions of interest from a certain reducing agent characterizes metal nanoparticle synthesis reactions. Therefore, a proposed mechanism will broadly involve a redox reaction.

1.4.1 *Proposed mechanism for nanoparticle formation*

Recently the first proposal was published that indicated the involvement of NADH and NADH-dependent enzymes in gold nanoparticle synthesis by microorganisms (He *et al.*, 2007). Figure 1.8 illustrates the proposed mechanism.

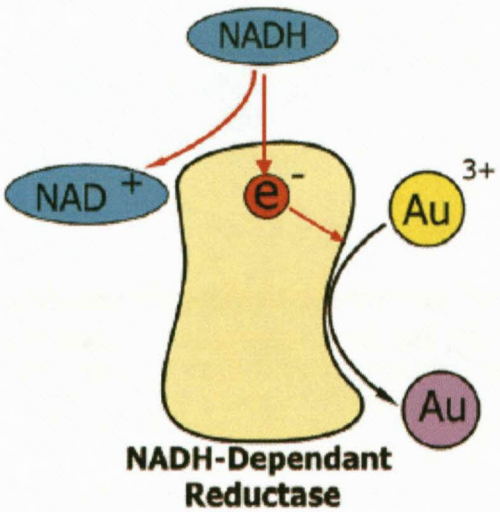

Figure 1.8: Proposed mechanism for gold bioreduction (Taken from He *et al.*, 2007).

As illustrated in Fig 1.8, the gold reduction system is possibly an electron shuttle in which gold ions act as a terminal electron acceptor. The gold ions are reduced to Au^0 and subsequently nanoparticles are formed. It is suggested that electrons are transferred from NADH by an NADH-dependent reductase, with the latter being an electron carrier. This mechanism does not describe either the enzyme involved or the native substrate of the enzyme.

1.5. Conclusions

The unique properties of metal nanoparticles are dependent on size and shape, development of technologies bases on the unusual physicochemical and optoelectronic properties of nanoparticles requires methods that can selectively produce specific shapes and sizes. The latter is elusive in chemical synthesis. Biological systems especially microoganisms have a potential of controlling the shape and size of nanoparticles.

The ability of microorganisms to synthesize nanoparticles seems not to be restricted exclusively to microorganisms isolated from environments containing metals in abundance. It therefore leaves the possibility of optimizing nanoparticle production by varying specific physical and chemical parameters. The availability of different microorganisms that produce nanoparticles of different morphologies could result in specifically tailored particles, with good monodispersity.

The mechanism with which this synthesis occurs is not yet elucidated and neither has the enzymes involved been characterized. The proposed mechanism does not provide answers to mechanistic aspects of nanoparticle formation, but holds potential for biological synthesis of these unique structures.

1.6 REFERENCES

Ahmad, A., Mukherjee P., Senapati S., Mandal D., Khan I. M., Kumar R. and Sastry, M. 2003a. Extracellular biosynthesis of silver nanoparticles using the fungus *Fusarium oxysporum. Colloids and surfaces B: Biointerfaces.*, **28:** 313 – 318

Ahmad, A., Senapati, S., Khan M. I., Kumar, R., Ramani, R., Srinivas V. and Sasstry. M. 2003b. Intracellular synthesis of gold nanoparticles by a novel alkalotolerant actinomycete. *Rhodococcus* species. *Nanotechnology.*, **14:** 824 – 828

Ahmand, A., Senapa, S., Khan I. M., Kumar, R. and Sastry, M. 2005. Extra-/ intracellular biosynthesis of gold nanoparticles by an alkalotolerant fungus, *Trichothecium* sp. *Journal of Biomedical Nanotechnology.*, ***1:*** 47 – 53

Antken R.J, Creely K.S. and Tran, C.L. 2004. Nanoparticles: An occupational hygiene review. *Health and Safety Executive, Research Report , 274*

Black, J. P, Ford, T. E. and Mitchell, R. 1986. The role of bacterial polymers in metal release into water. pp. 37 – 42. In: Cullimore R. (ed). International symposium on biofouled aquifers: prevention and restoration Bethesda, MD Awara,

Carrot, G., Valmalette, J. C., Plummer, C. J. G., Scholz, S. M., Dutta, J., Hofmann H. and Hilborn, J.G. 1998. Gold nanoparticle synthesis in graft copolymer micelles. *Colloid and Polymer Science.*, **276:** 853 – 859

Chanmugathas, P. and Bollag, J.M. 1988. A column study of biological mobilization and speciation of cadmium in soil. *Archives of Environmental Contamination and Toxicology (New York, NY).*, **7:** 229 – 237

Coughlin, R. T., Tonsager, S. and McGroarty, E.J. 1983. Quantitation of metal cations to membranes and extracted lipopolysaccharides from *Escherichia coli. Biochemistry.*, **22:** 2002

Dietrich, R.C., Young, I.T. and Garini, Y. 2005. Gold nanoparticles: A novel application of spectral imaging in proteomics–Preliminary results. *Proceedings of International Society of Optical Engeenering.*, **5694:** 82 – 89

Doyle, R. J. 1989. How cell walls of gram-negative bacteria interact with metal ions. pp. 275 – 293. In: Beveridge T .J., Doyl R. J. (eds.), *Metal ions and bacteria.*. Wiley, New York

Ehrlich, H.L. 1997. Microbes and metals. *Applied Microbiology and Biolotechnology.*, **48:** 687 – 692

Ford, T. and Ryan, D. 1995. Toxic metals in aquatic systems: A microbiological perspective. *Environmental health perspective.*, **103:** 25 – 28

Fortina, P., Kricka, L.J., Surrey, S. and Grodzinski, P. 2005. Nanobiotechnology: the promise and reality of new approaches to molecular recognition. *Trends in Biotechnology.*, **23:** 168 – 173

Frank, S., Poncharal, P., Wang, Z. and de Heer, W. 1998. Carbon nanotube quantum resistors. *Science.*, **28:** 1744 – 1746

Gadd, G.M. 1993. Microbial formation and transformation of organometallic and organometalloid compounds. *Federation of European Microbiological Societies Microbiology Reviews.*, **11:** 297 – 316

Gadd, G.M. 1996. Influence of microorganisms on the environmental fate of radionuclide. *Endevour.*, **20:** 150 – 156

Gadd, G.M. and Sayer, J.A. 2000. Influence of fungi and environmental mobility of metals and metalloids. Influence of Fungi on the Environmental mobility of Metals and Metalloids. pp. 237 – 256. *In*: Lovely D.R (ed), Environmental Microbe-metal interactions, *American Society for Microbiology Press*, Washington, D. C,

Gorby, Y.A., Beveridge, T.J. and Blakemore, R.P. 1988. Characterization of magnetosomes membrane. *Journal of Bacteriology.*, **170:** 834 – 841

Grieve, K., Mulvaney, P. and Grieser, F. 2000. Synthesis and electronic properties of semiconductor nanoparticles/quantum dots. *Current Opinion in Colloids and Interface Science.*, **5:** 168 – 172

Haes, A., Stuart, D., Nie, S. and Van Duyne, R. 2004a. Using solution phase nanoparticles, surface – confined nanoparticles arrays and single nanoparticles as biological sensing platforms. *Journal of Fluorescence.*, **14:** 355 – 367

Haes, A., Hall., W ., Chang., L ., Klein., W. and Van Duyne., R. 2004b. A localized surface plasmon resonsnce biosensor. First steps towards Alzheimer's disease. *Nanotechnology Letters.*, **4:** 1029 – 1034.

Han, M., Gao, X., Su, J.Z. and Nie, S. 2001. Quantum-dot tagged microbeads for multiple optical coding of biomolecules. *Nature Biotechnology.*, **19:** 631 - 635

He, S., Guo, Z., Zhang, Y., Wang, J. and Gu, N. 2007. Biosynthesis of gold nanoparticles using the bacteria *Rhodopseudomonas* capsulate. *Material Letters.*, **61**: 3984 – 3987

Huang, W., Qian, W. and El-Sayed, A. 2005. Optically detected coherent picosecond lattice oscillations in two dimensional arrays of gold nanocrystals of different sizes and shapes induced by femto second laser pulses. *Proceedings of International Society of Optical Engineering.*, **5927:** 592701 – 592709

Ibrahim, Z., Ahmad, W. A. and Baba, A.B. 2001. Bioaccumulation of silver and isolation of metal binding protein from *P. diminuta. Brazilian Archives Biology and Technology.*, **44:** 223 -225

Iijima, S. 1991. Helicalmicrotubeles of graphitic carbon. *Nature.*, ***354:*** *56 – 58*

Ingledew W.J. 1982. Thiobacillus ferrooxidans. The bioenergetics of an acidophilic chemolithotroph. *Biochimica et B*iophysica *Acta.*, **683:** 89 – 117

Jorter, J. and Rao, C.N.R. 2002. Nanostructured advanced materials. Perspective and directions. *Pure and Applied Chemistry.*, **74:** 1491 – 1506

Kashefi, K., Tor, J.M., Nevin K.P. and Lovely, D.R. 2001. Reductive precipitation of gold by dissimilatory Fe^{3+}-reducing bacteria and archaea. *Applied and Environmental Microbiology.*, ***67:*** *3275 – 3279*

Klaus, T., Joerger, R., Olsson, E. and. Granqvist.,C. G. 1999. Silver-based crystalline nanoparticles, microbially fabricated. *Proceedings of National Academy of Sciences of the United States of America.*, **96:** 13611 – 13614

Kowshik, M., Deshmunkh, N., Vogel, W., Urban, J., Kulkarni, S.K. and Paknikar, K.M. 2001. Microbial Synthesis of Semiconductor CdS Nanoparticles, Their Characterization, and use in the Fabrication of an Ideal Diode. *Biotechnology and Bioengineering.*, **78:** 583 – 588

Kumar, A., Joshi, H.M., Mandale, A.B., Seivastava, R., Anyanthanya, S.D., Pasricha, R. and Sastry, M. 2004. Phase transfer of platinum nanoparticles from aqueous to organic solutions using fatty amine molecules. *Journal of Chemical Science.*, **116:** 293 – 300

Langley, S. and Beveridge, T.J. 1999. Effects of O-side- chain-lipopolysaccharide chemistry on metal binding. *Applied and Environmental Microbiology.*, **65:** 489 – 498.

Liu, G., Xu, S. and Qian, Y. 2000. Nanofabrication of self assembly monolaryers using scanning probe lithography. *Accounts of Chemical Research.*, **33:** 457 – 466

Lowenstam, H.A. and Weiner S. 1989. Biomineralization. Oxford University Press, New York Mann S, Webb J. and Williams, R.J.P (Eds), 1989. Biomineralization: *Chemical and Biochemical Perspectives*, VCH Publishers, New York, 325

Lovley, D.R. and Phillips, E.J.P. 1988. Novel mode of microbial energy metabolism: organic carbon oxidation coupled to dissimilatory reduction of iron or manganese. *Applied Environmental Microbiology.*, **54:** 1472 – 480

Lovely, D.R. 1990. Magnetite formation during microbial dissimilatory iron reduction. *Iron Biominerals*, Plenum Press, New York.151 – 66

Mann, S., Sparks, N.H.C. and Wade, V.J. 1990a. Crystallochemical control of iron oxide biomineralization. pp. 21 – 9. In: R. B. Frankel and R. P. Blakemore (eds.). *Iron Biominerals.* Plenum Press, New York, United States of America

Mann, S., Sparks, N.H. C., Frankel, R. B., Bazylinski, D. A. and Jannasch H.W. 1990b. Biomineralization of ferromagnetic greigite (Fe_3O_4) and iron pyrite (FeS_2) in a magnetotactic bacterium. *Nature.*, **343:** 258 – 260

Maynard, D. A., Baron, P.A., Foley, M., Shevedova, A.A., Kisin, E.R. and Castranova V. 2004. Exposure to carbon nanotube material: Aerosol release during realease during the handling of unrefined single walled carbon nanotube material. *Journal of Toxicology and. Environmental Health.*, **1:** 87 – 107

Morley, G.F., Sayer, J.A., Wilkinson, S.C., Garhieb, M.M. and Gadd G.M. 1996. Fungal sequestration, solubilization and transformation of toxic metals. pp, 235 – 256. *In* J.C Frankland, Mugan, N. and Gadd., G. M.(eds.), *Fungi and Environmental Change. Cambridge* University Press, Cambridge, United Kingdom.:

Mukherjee, P., Ahamad, A., Manda, D. Senapati, S., Sainkar, R.S., Khan, M.I., Ramani, R., Paricha, R., Ajayakumar, P.V, Alam, M., Sastry, M. and Kumar, R. 2001. Bioreduction of $AuCl_4^-$ ions by fungus, *Verticillium* sp. and Surface trapping of the gold nanoparticles formed. *Angewandte Chemie International Edition.*, **40:** 3585 – 3588

Nair, B. and Pradeep, T. 2002. Coalescence of nanoparticles and formation of submicron crystallites assisted by *Lactobacillus* strains. *Crystal Growth and Design.*, **2:** 293 – 298

Nie, D.H. 1999. Microbial heavy-metal resistance. *Applied Microbiology and Biotechnology.*, **51:** 730 – 750

Oremland, R. S., Hollibaugh J. T., Maest A. S., Presser T. S, Millet L. and Culbertsons, S. 1989. Selenate reduction by anaerobic bacteria in sediments

and culture biogeochemical significance of a novel sulfate independent respiration. *Applied Environmental Microbiology.*, **55:** 2333 – 2343

Okuda, Y., Denda K. and Fukumori, Y. 1996. Cloning and sequencing of a gene encoding a new member of the tetratricopeptide protein family from magnetosomes of *Magnetospirillum magnetotacticum. Gene.*, **171:** 99 – 102

Ortiz, D. F., Rucsitti, T., McCue, K. F. and Ow D. W. 1995. Transport of metal binding peptide by HMT-1, a fussion yeast ABC type vacuolar membrane protein. *Journal of Biological Chememistry.*, **270:** 4721 – 4728

Pal, U., Loaiza-Gonzalez, G., Bautista-Hernández, A. and Vázquez-Cuchillo. 2000. Synthesis of CdS nanoparticles through colloidal route. *Superficiesy Vacio.*, **11:** 40 – 43

Schüler, D. and Baeuerlein, D. 1997. Iron uptake and magnetite crystal formation of the magnetic bacterium *Magnetospirillum gryphiswaldense.* pp, 159 – 185. *In*: Winkelmann and C. J. Carrano (ed.), Transition metals in microbial metabolism. Harwood Academic Publishers, Amsterdam, The Netherlands

Schüler, D. and Baeuerlein, D. 1998. Dynamics of Iron Uptake and Fe_3O_4 Biomineralization during Aerobic and Microaerobic Growth of *Magnetospirillum gryphiswaldense. Journal of Bacteriology.*, **180:** 159 – 162

Schüler, D. 1999. Formation of magnetosomes in magnetotactic bacteria. *Journal of Molecular Microbiology and Biotechnology.*, **1***: 79 – 86*

Shanker, S.S., Ahamad, A., Paricha. R. and Sastry, M. 2003. Bioreduction of chloroaurate ions by geranium leaves and its endophytic fungus yields gold nanoparticles of different shapes. *Journal of Materials Chemistry.*, **13:** 1822 – 1826

Shi, L., Tiwari, S., Rana, F. and Chan, K. 1996. Single charge and confinement effects in nano-crystal memories. *Applied Physics Letters.*, **69:** 1232 – 1234

Slawson, R.M., Trevors, J.T. and Lee, H. 1992. Silver accumulation and resistance in *Pseudomonas stutzeri. Archives of Microbiology.*, **158:** 398 – 404

Stanley, B., Mehmet, S. and Erik, J. 2000. A genetic analysis of crystal growth. *Journal of Molecular Biology.*, **299:** 725 – 735

Sun, Y. and Xia, Y. 2002. Shape controlled synthesis of gold and silver nanoparticles. *Science.*, **298:** 2176 – 2178

Treacy, M., Ebbesen. T. and Gibson, J. 1996. Exceptionally high Young's modulus observed for individual carbon nanotubes. *Nature.*, **381:** 678 – 680

White, C., Sayer, J.A. and Gadd, G.M. 1997. Microbial solubilizationand immobilization of toxic metals: key biogeochemical processes for treatment of contamination. *Federation of European Microbiological Societies Microbiology Reviews.*, **20:** 503 – 516

Whitesides, G.M. 2003. Right "size" in nanobiotechnology. *Nature Biotechnology.*, **21:** 1161 – 1165

Xue, H.B., Stumm, W. and Sigg, L. 1988. The binding of heavy metals to algal surfaces. *Water Research.*, **22:** 917 – 926

Zhang, W., Qiao, X. and Chen, J. 2007. Synthesis of silver nanoparticles—Effects of concerned parameters in water/oil microemulsion. *Materials and Science Engineering:B.*, **142:** 1 – 15

Chapter 2

Screening of Yeast species for nanoparticle synthesis

2.1 Introduction

It is well known that microoganisms can synthesize metal nanoparticles (Lowenstam and Weiner, 1989; Lengke and Southam, 2006), for example the formation of placer gold by bacteria (Southam and Beveridge, 1994). Several bacterial strains have been reported to form nanoparticles intracellularly. The silver tolerant bacterial strain *Pseudomonas dimuta* was reported to form silver nanoparticles resulting in nanoparticle accumulation intracellularly (Ibrahim *et al.*, 2001). Furthermore, bacteria not normally exposed to high concentrations of metal ions have been used to form nanoparticles. Nair and Pradeep (2002) used *Lactobacillus* strains isolated from butter milk to form both silver and gold nanoparticles. The ability of bacteria to form nanoparticles could be linked to specific mechanisms of tolerance, which include efflux systems, alteration of solubility and toxicity by changes in the redox state of the metal ions (Gadd and Sayer, 2000; Silver, 1996). These tolerance mechanisms also apply to fungi.

It has been observed that an alkalothermophillic actinomycete, *Thermonospora* sp. when incubated with gold ions, reduced metal ions extracellularly, resulting in polydispersed gold nanoparticles (Ahmad *et al.*, 2003a). In contrast, intracellular synthesis of gold nanoparticles occurs in *Rhodococcus* sp. (Ahmad *et al.*, 2003b), where particles are more concentrated on the cytoplasmic membrane than the cell wall. The use of fungi in synthesis of nanoparticles is new compared to that of bacteria. Exposure of *Verticillium* sp. to silver and gold ions resulted in the intracellular formation of silver and gold nanoparticles respectivelly (Mukherjee *et al.*, 2001a,b). The ability of *Verticillium* cells to multiply after exposure to metal ions illustrated the potential of using microoganisms in the synthesis of nanomaterials (Mukherjee *et al.*, 2001b). Recently, it was shown that biomass of *Fusarium oxysporum* formed highly stable Au-Ag alloy

nanoparticles when incubated with equal molar solutions of $HAuCl_4$ and $AgNO_3$. Variation in the amount of biomass revealed that secreted cofactor NADH plays an important role in determining the composition of Au-Ag alloy (Senapati *et al.*, 2005). Earlier Ahmad *et al.* (2002) reported on the extracellular synthesis CdS quatum dots using *F. oxysporum*. In the same study, reaction of fungal biomass with aqueous $CdNO_3$ for an extended period of time did not yield CdS nanoparticles, and was thought to result from the release of a sulphate reductase enzyme into the solution.

CdS and other semiconductor nanoparticle biosynthesis were observed in yeast earlier than in filamentous fungi. Exposure of *Candida glabrata* to cadmium ions led to intracellular formation of CdS quatum dots (Reese and Winge, 1988). Furthermore, *Torulopsis* sp. is capable of synthesizing PbS nanoparticles when exposed to Pb ions (Kowshik *et al.*, 2002a). The PbS nanoparticles were extracted by freeze-thawing and characterized by sharp absorbance maximum at 330 nm. Kowshik and co-workers (2002b) have shown synthesis of CdS by *Schizosaccharomyces pombe* yeast. Though yeasts have been shown to synthesize nanoparticles intracellularly, very recently their use in producing silver nanoparticle has been seen, by a silver tolerant strain MKY3 (Kowshik *et al.*, 2003). Particles with a 2-5 nm size range were formed when exposed to silver ions in the exponential phase of growth.

Thus, an aim of this study is to screen various yeast species in the MIRCEN (Microbiological Resource Centre) at UFS culture collection for the ability to produce or aid in gold nanoparticle formation.

2.2 Materials and Methods

2.2.1 *Yeast growth conditions*

With the help of MIRCEN staff at UFS and literature associated with research conducted on the culture collection, different isolates were chosen for screening. In literature most metal reducing microoganisms were isolated from soil. Thus screened yeast species in this work were isolated from soil. Yeasts were routinely cultured in nutrient broth YM (Yeast Malt extract) and on nutrient agar plates (YM). The media (YM) contains: yeast extract (6 g/l), malt extract (6 g/l) and peptone (10 g/l), pH 7.0. Cultures were incubated at 25°C and agitated at 150 rpms. Growth was monitored by measuring the O.D (690nm) over time, in 50 ml growth media in 500 ml Erlenmeyer flask. However, O.D was also converted to dry biomass using a standard curve.

2.2.2 *Biosynthesis of gold nanoparticles for initial screening*

Cultures were inoculated from plates, grown in test tubes containing 10 ml YM medium at 25°C and agitated at 150 rpms. After 24 hours incubation the biomass was separated from the medium by centrifugation (10 000 *x g*, 5 min) and washed three times with 0.8% (w/v) sodium chloride solution.

Nanoparticle formation was assessed by adding different concentrations $HAuCl_4$ (0.1 mM, 0.5 mM and 1 mM) to a 2.0 ml cell suspension with optical density readings measured at 690 nm and adjusted to 1.0 optical density unit for standardization. Incubation was done at 25°C and agitated at 150 rpms, with evaluation of nanoparticle formation taking place every 24 hours. The accumulation and reduction of gold were followed by visual observation of the biomass turning red or purple, conveniently indicating gold nanoparticle or nanoparticle aggregates formation (Mukherjee *et al.*, 2001b). This visualization was later quantified using UV-Vis spectral analysis.

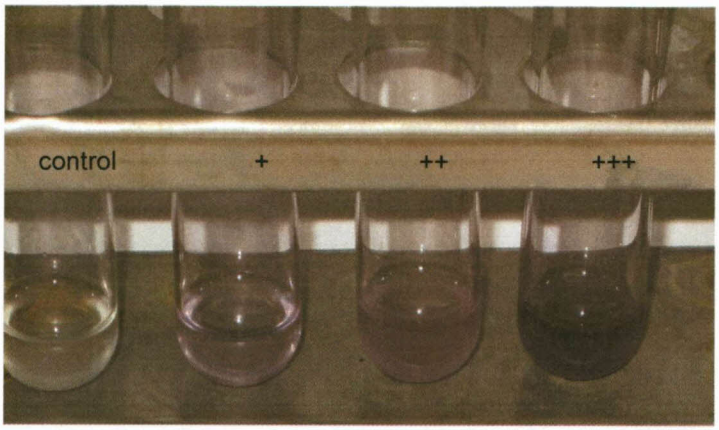

Figure 2.1: Colour intensity ratings for gold nanoparticles in solution, indicated by number of + signs.

2.2.3. *Gold reduction assays*

Whole cells (O.D 1.0 unit at 690 nm) were suspended in 20 mM acetate buffer (pH 5.0), to which 0.5 mM $HAuCl_4$ were added, this working concentration was found to be optimum for gold reduction as seen in table 2.1.

2.2.3.1 *Ethopropazine Hydrochloride (EPH) assay*

The whole cell biomass was separated from the gold ion containing solution by centrifugation (10 000 *x g*, 10 min, 4°C). The amount of $HAuCl_4$ in solution was deduced from the calibration curve, constructed using a method taken from Melwanki *et al.* (2002). This assay is a colorimetric assay, where $HAuCl_4$) forms a complex with EPH and the resulting complex absorbs maximally at 513 nm. A standard curve was constructed for the linear range of $HAuCl_4$ concentration (Figure 2.2).

The supernatant (0.5 ml) containing gold ion solution was added to 10 M phosphoric acid (2.0 ml) and 0.2% (v/v) EPH (1.0 ml). The reaction volume was adjusted with water to a final volume of 5 ml and the absorbance measured at 513 nm.

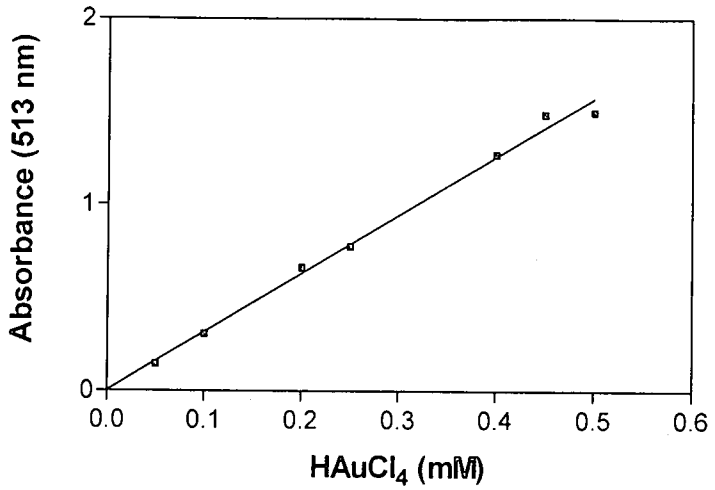

Figure 2.2: Standard curve for assay of gold ion removal. Standard deviations for triplicate determination are smaller than symbols used for the data points. $R^2 = 0.9936$

2.2.3.2. *Phloxine assay*

Another option to determine $HAuCl_4$ ions concentration is the phloxine assay described by Fujita *et al.* (1999). The following components were mixed in a test tube to a final volume of 1 ml: 100 µl sample containing gold ions, 50 µl of 0.5% methylcellulose, 100 µl of 0.1 mM thiamine solution, 200 µl of 0.05 M disodium ethylenediaminetetraacetate (EDTA), 100 µl of 0.001 mM phloxine solution, 450 µl distilled water. The mixture was then incubated in a 40°C water bath for 20 min, after which the solution was cooled for 5 min at room temperature and the absorbance of the resultant solution measured at 565 nm against a blank that was prepared in the same way, except that no gold ions were added. $HAuCl_4$ forms a complex with phloxine and thiamine, and absorbs maximally at a wavelength of 565 nm.

Fujita and co-workers, 1999, however measured the absorbance of the phloxine-gold complex at 570 nm. After a wavelength scan and standard curve evaluation the wavelength was adjusted to 565 nm (Figure 2.3). This adaptation was especially important at very low concentrations of $HAuCl_4$. The standard curve was then constructed at 565 nm (Figure 2.4).

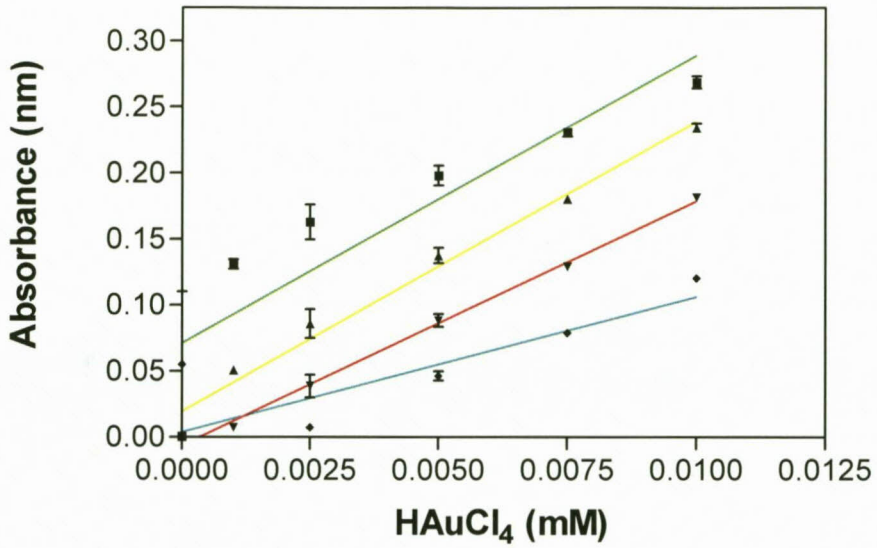

Figure 2.3: Standard curve for gold ion removal at different wavelengths and R^2 values, 555 nm (■) 0.7969, 560 nm (▲) 0.9728, 565 nm (▼) 0.9884 and 570 nm (♦) 0.4239. Error bars indicate standard deviation.

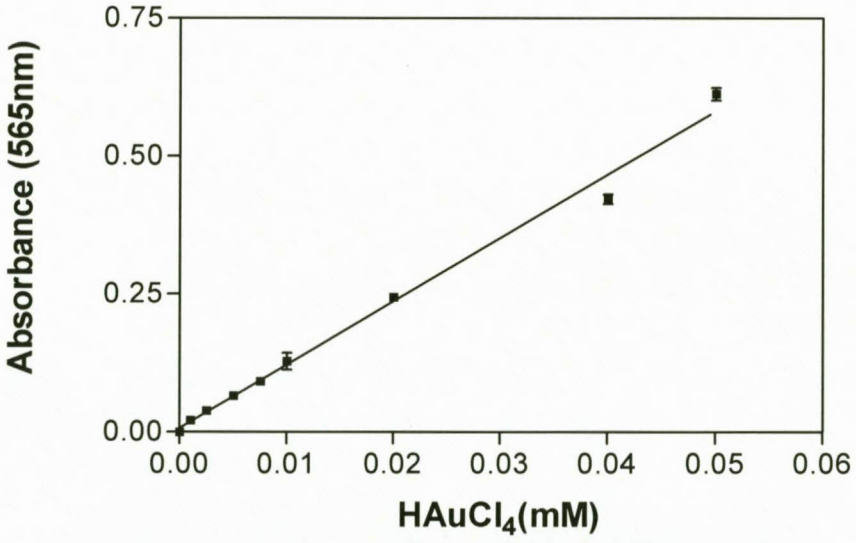

Figure 2.4: Standard curve for the assay of gold ion removal using the phloxine assay with a R^2 value of 0.9883. Error bars indicate standard deviation.

2.2.4. *Transmission electron microscopy*

TEM was done to visualize nanoparticles within whole cells' cross-sections. The cells were fixed for one hour in a 3% glutaraldehyde solution, prepared in sodium phosphate buffer, pH 7.0. Cell recovery was done by centrifugation and washing twice with sodium phosphate buffer, pH 7.0. No secondary fixation was done, as OsO_4 would have interfered with the analysis. The fixated cells were mixed with molten 1% agar and placed drop-wise on clean microscope slides. Once the droplets were solidified it was cut into small pieces and dehydrated with a series of 50-90% acetone for 30 minutes followed by a 100% acetone step for 1 hour followed by another 100% acetone step left overnight.

Epoxy resin was prepared freshly at the onset of the final dehydration step, by weighing (not volumetric measuring) of the following components: 23 g VCD (vinylcyclohexene dioxide), 62 g NSA (nonenyl succinic anhydride), 14 g DER736 (diglycidyl ether of polypropylene glycol) and 1 g DMAE [(S1) dimethylaminoethanol] added together with constant stirring. All but approximately 1 ml of the remaining 100% acetone was decanted and to this 1 ml of epoxy was added. The mixture was stirred well and allowed to impregnate the samples for up to 8 hours. The 1:1 mixture (epoxy: ethanol) was then removed and replaced by 1 ml epoxy and this step repeated again overnight. The samples were then placed in a desiccator to remove all traces of the acetone.

The moulds were dried in an embedding oven overnight. Samples and epoxy were transferred to the pre-dried and pre-heated moulds and allowed to polymerize at 70°C for eight hours. Two days after polymerization the embedded material was sectioned by ultra-microtome, yielding sections of approximately 0.2 µm. Sections were mounted on copper grids and electron micrographs were taken with a Joel 6400 WINSEM (Japan) and a Philips CM 100 (The Netherlands) TEM (Van Wyk and Wingfield, 1991).

2.3 Results and Discussion

2.3.1 *Screening*

Different yeast species were screened for their ability to reduce $HAuCl_4$ and produce gold nanoparticles as described in section 2.2.2. Some yeast species are reported to form nanoparticles intracellularly (Mukherjee *et al.,* 2001b), thereby resulting in the biomass turning purple and not the solution. The time taken for the biomass to turn purple, as well as the colour intensity, was used to select for those organisms that gave positive reduction results (Table 2.1). This screening was done with whole cell preparates.

Table 2.1. Screening results of gold reduction and nanoparticle formation by different yeast species

Yeast Species	0.1 mM	0.5 mM	1 mM	Time(h)
Debaryomyces hansenii UOFSY-*0610*	-	-	-	144
Cryptococcus macerans UOFSY-*1352*	+++	++	-	144
Kluveromyces lactis UOFSY-*1167*	++	+	-	144
Candida glabrata UOFSY *-0791*	+	-	-	144
Saccharomyces cerevisiae UOFSY-*2169*	+	-	-	120
Pichia jadinii UOFSY-*0156*	+	-	-	120
Pichia jadinii UOFSY-*0520*	+	-	-	120
Aursobasidium pullulans NRRLY2311-1	++	+++	-	48
Lipomyces starkeyi UOFSY-1999	+	++	-	48
Candida palmiophila UOFSY-2554	+++	-	-	144
Candida palmioleophila UOFSY-2551	++	+++	-	120
Debaryomyces nepalensis UOFSY-2552	-	-	-	144
Candida viswanathii UOFSY-2553	+	+++	-	72
Candida viswanathii UOFSY-2555	+	+++	-	144
Candida palmioleophila UOFSY-2556	+	+++	-	144
Candida viswanathii UOFSY-2557	+	++	-	144
Schizosaccharomyces pombe UOFSY-2174	-	-	-	144
Candida viswanathii UOFSY-2558	+	++	-	48
Cryptococcus keutzingii UOFSY-2564	-	-	-	96
Candida palmioleophila UOFSY-2568	++	+++	-	96

Rhodotorula graminis UOFSY-1623T	+++	++++	+	48
Candida viswanathii UOFSY-1296	+++	++++	+	48
Arthroascus javanensis UOFSY-1251	++	-	-	48
Arxiozyma telluris UOFSY-1213	++	-	-	48
Arxula adeninovorans UOFSY-1224T	-	-	-	48
Geotrichum fermentans UOFSY-1026	++	++++	+	48
Metschikowia pulcherima UOFSY-1076	+	-	-	72
Myxozyma geophila UOFSY-1596	+	-	-	72
Hanseniaspora vineae UOFSY-0151T	-	-	-	72
Nadsonia commutata UOFSY-2332	-	-	-	72

+ indicates amount of colloidal gold formationn observed which is directly proportional to colour intensity *(section 2.2.2)*

- sign indicates zero colloidal gold

The first specie to show reduction was *Cryptococcus macerans* UOFS Y-1352 after 144 hours for both 0.1 and 0.5 mM $HAuCl_4$. A significant difference was observed later between *Aursobasidium pullulans* NRRLY 2311-1 and *Cryptococcus macerans* UOFS Y-1352. The former was able to reduce gold within a shorter time. With further screenings, species that resulted in good reduction at both 0.1 mM and 0.5 mM $HAuCl_4$ concentration in the shortest time were selected for further studies namely *Rhodotorula graminis* UOFS Y-1623T, *Candida viswanathii* UOFS Y-1296 and *Geotrichum fermentans* UOFS Y-1026.

2.3.2 *Growth studies and removal of $HAuCl_4$ ions in solution*

Growth analysis of the selected three yeast species was done and monitored as described in section 2.2.1, however the $HAuCl_4$ concentration used was 0.5 mM. Figure 2.5 shows growth profiles of the selected yeast. The ability of cells harvested in exponential and stationary phase were evaluated for gold reduction (Table 2.2). The comparisons were made with equal amount (3 mg/ml) of cells as described in section 2.2.2.

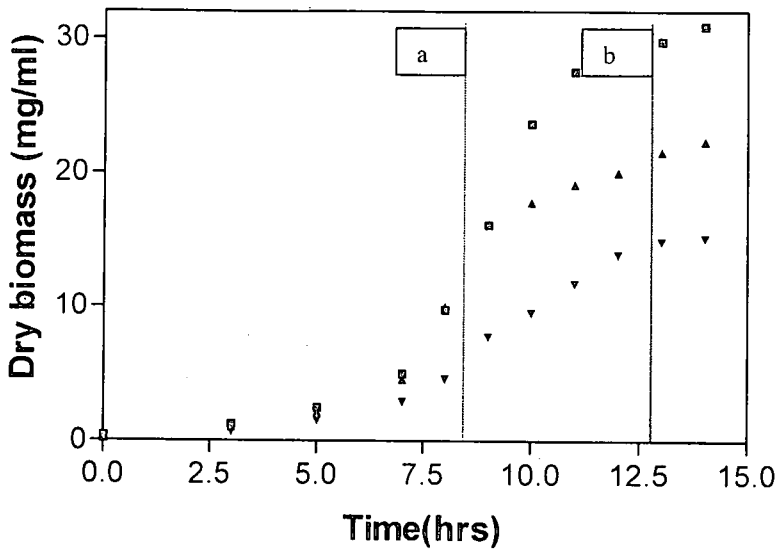

Figure 2.5: Growth studies of *C. viswanathii* (▫), *G. fermentans* (▲) and *R. graminis* (▽). Exponential phase (a) and stationary phase (b).

Table 2.2 Removal of $HAuCl_4$ by standardised biomass in exponential phase and stationary phase

Yeast Species	***Au (%) Removed/Reduced***		***Time (h)***
	Exponential Phase	*Stationary Phase*	
C. viswanathii	*15.83*	*23.29*	*24*
G. fermentans	*52.40*	*82.23*	*24*
R. graminis	*55.93*	*58.33*	*24*

- Rates were determined using EPH assay

Incubation of biomass from stationary phase with 0.5 mM $HAuCl_4$ concentration resulted in higher concentration of $HAuCl_4$ removed compared to biomass in exponential phase (Table 2.2). Sweeney *et al.* (2004) reported a 20-fold increase of CdS nanoparticle formation by *E. coli* cells harvested in stationary phase compared to those harvested in late exponential phase. *G. fermentans* reduced most gold ions in a 24 hours incubation period. *C. viswanathii* was the least effective of the three yeast species in removing $HAuCl_4$ from solution. *G. fermentans* also showed a higher gold ion removal rate (Table 2.3) and was the most promising candidate for gold reduction.

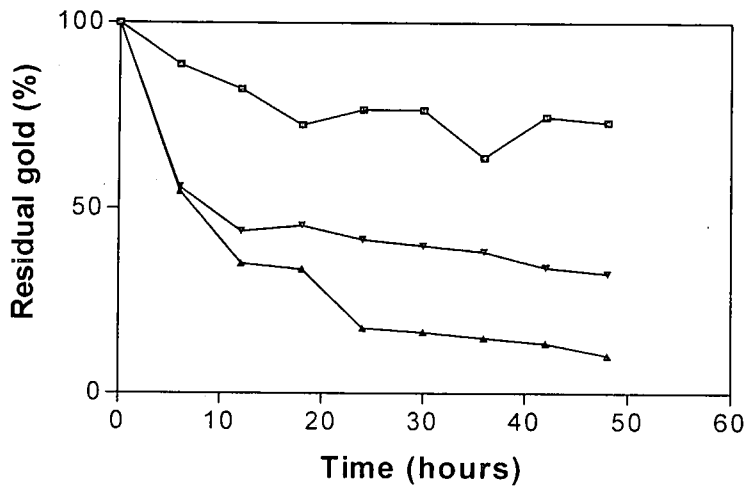

Figure 2.6: $HAuCl_4$ removal by yeast cells that were harvested at stationary phase. *C. viswanathii* (■), *G. fermentans* (▲) and R. *graminis* (▼).

Table 2.3 The rate of $HAuCl_4$ removal by biomass in stationary phase

Yeast Species	*Rate of $HAuCl_4$ removal (h^{-1})*
C. viswanathii	1.52
G. fermentans	3.2
R. graminis	1.98

Fungal metal uptake is essentially a biphasic process consisting of a metabolism-independent and metabolism-dependent step. The initial biosorption step is rapid (Avery and Tobin, 1992; Brady and Duncan, 1994), typically only a few minutes in duration (White and Gadd, 1987) and is independent of temperature (Mowll and Gadd 1984). Biosorption is exclusively responsible for metal accumulation by non-viable biomass (Tobin *et al.,*1984; Avery and Tobin, 1992) owing to the absence of metabolic activity necessary for intracellular metal accumulation. The second step, designated bioaccumulation, is a slower metabolism-dependent step, influenced by factors such as temperature and the presence of metabolic inhibitors (deRome and Gadd 1987; Mowll and Gadd, 1984). Greater amounts of metal may be accumulated by this means in some organisms, especially yeasts (Avery and Tobin, 1992).

When active biomass of the selected strains was incubated with 0.5 mM gold $HAuCl_4$, the rate at which $HAuCl_4$ was removed in solution was highest in *G. fermentans,* followed *by R. graminis* and least in *C. viswanathii* (Table 2.3). There was a rapid disappearance of gold ions for approximately the first six hours of incubation, which subsided over time. Because of the high $HAuCl_4$ ion removal rate, *G. fermentans* was selected for further study; rates were calculated from the linear part of the graph in Figure 2.6.

The initial removal may be due to adsorption of ions to the cell wall as opposed to direct uptake and reduction. Here, possibly gold ion binding sites in each of the strains have different points of saturation. When binding sites are saturated a

decrease in $HAuCl_4$ removal is eminent. Results obtained with $HAuCl_4$ ion removal by the above-mentioned yeasts are in agreement with findings that metal cations could profoundly influence the nature of microoganism's cell wall as well as its electrical characteristic, and type of metal binding to the cell wall is a function of the external accessibility of metal ion species and the strength of binding (Beveridge and Murray, 1976).

The results in this study demonstrate a definite interaction of yeasts and $HAuCl_4$ (Au^{3+}) that result in gold nanoparticle formation. However, not all yeasts have this capacity. Because the initial soluble gold was the auric cation (Au^{3+}), reducing power is necessary to form elemental gold. Thus, the removal of $HAuCl_4$ could indicate reduction. Gold is a biologically inessential metal and in the ionic state, is a strong oxidizing agent and displays some microbiocidal properties (Sadler, 1976; Southam *et al.,* 2000). Although some microoganisms can use complexation to remove toxic gold ions, the most wide spread mechanism of protection appears to be the reduction of the ionic gold to the elemental state (Korobushkina *et al.,* 1989). Interesting to observe in this study is that nanoparticles were not formed at 1 mM $HAuCl_4$ when whole cells were used. This suggests lack of gold ion tolerance at this concentration. Optimum $HAuCl_4$ concentration for nanoparticle formation was 0.5 mM as indicated on (Table 2.1).

2.3.3 *Optimizing physicochemical parameters for gold nanoparticle formation*

The optimum growth temperature for these yeast species is around 25 °C (de Hoog *et al.,* 1998; Fell and Statzell-Tallman, 1998), however, even though nanoparticle formation occurred at this temperature, one could significantly increase the rate of nanoparticle formation by increasing temperature (Figure 2.7). Nanoparticles formed at high temperatures were bigger in size compared to the ones formed at low temperature. However, increasing temperature might

result in uncontrolled nanoparticle formation, amorphous nanoparticles were frequently observed. At lower temperatures, smaller particle were formed in abundance (Figure 2.7) (Gericke and Pinches, 2006).

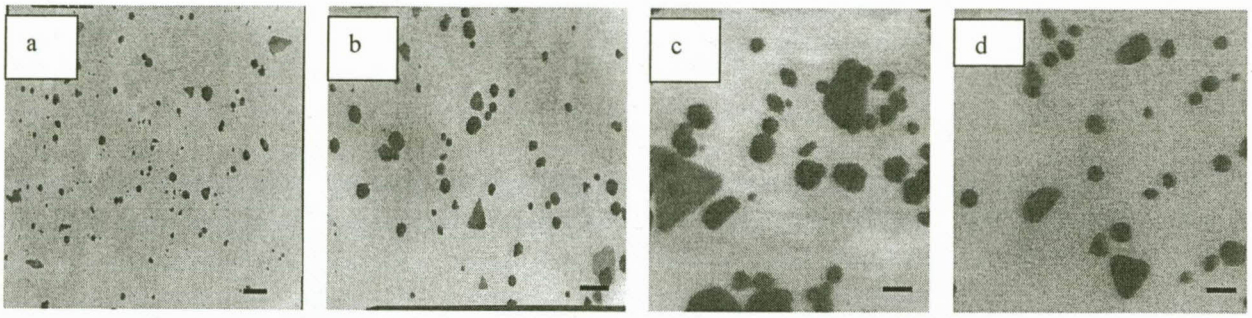

Figure 2.7: TEM micrographs of gold nanoparticles formed by *Verticillium sp.* cells exposed to gold ions at different temperature (a) 25 °C, (b) 35 °C, (c) 50 °C and 70 °C. The scale bar is 100 nm. (Taken from Gericke and Pinches, 2006).

It is clear that physicochemical parameters will greatly influence the nanoparticle formation. Evaluation of this factor at protein level is presented in Chapter 3, especially if this is mediated by an enzymatic reduction.

Gericke and Pinches (2006) also showed the particles formed at pH 3 were predominantly spherical in shape, relatively uniform in size, with the majority of the particles less than 10 nm in diameter. Nanoparticles synthesised at pH 5 included small spherical particles, similar to those dominating at pH 3. In addition, a large number of bigger particles with well-defined shapes, including pseudo-triangonal octahedral, hexagonal octahedral, spheres and rods also occurred at this pH. The shapes of the particles formed at pH 7 were similar to those formed at pH 9 and included small spherical particles as well as bigger particles with irregular, undefined shapes. Lower numbers of particles per cell were present at pH 9 than at pH 7 (Gericke and Pinches, 2006). Thus pH was also considered as variable parameter in Chapter 3.

In section 2.2.3 we describe the use of acetate buffer with whole cell reduction experiments, this was an important change from literature since blank rates were reported with some buffers.

2.3.4 *TEM analysis of whole cells incubated with 0.5 mM $HAuCl_4$*

Evaluation of the gold nanoparticles was also done by TEM, nanoparticle distribution is predominantly in the cytoplasm with one or two particles associated with the membranes (Figure 2.8).

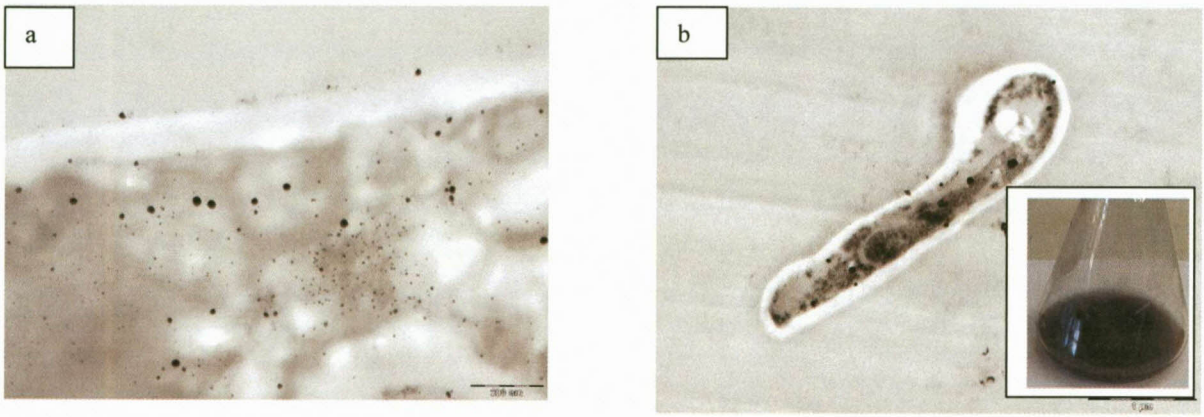

Figure 2.8: TEM micrograph of the thin cross section of G. *fermentans (a)* the scale bar is 200 nm and (b) the scale bar is 1000 nm. The insert is a picture of the hetergemous gold nanoparticles formed by the culture.

The cells in the above micrograph are assuming unusual shapes due to lack of preservation in structural integrity since no secondary fixation was done. However, the particles formed and their distribution is consistent in all cells. TEM analysis of cells that were incubated with gold ions indicated the site of nanoparticle formation in *G. fermentans* to be the cytoplasm and the exterior part of the cell envelope. However, in *C. viswanathii,* nanoparticles were observed in both the cytoplasm and the surrounding environment (Figure 2.9).

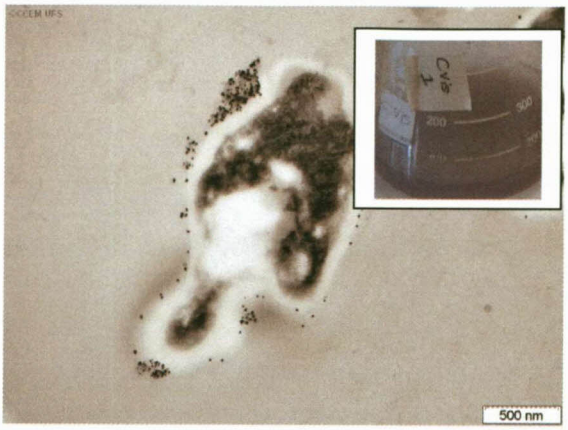

Figure 2.9: TEM micrograph of the thin cross section of *C. viswanathii (a)* the scale bar is the scale bar is 500 nm. The insert is a picture of the gold nanoparticles formed by the culture.

This finding extends earlier observations of Ahmand *et al.,* (2003a,b). Microoganisms can transport metal ions into the cytoplasm, where reduction of the metal can then follow and/or secrete enzymes or other organic molecules to reduce metals extracellularly.

2.3.5 *Energy dispersive spectra*

EDS spectra generated by the whole cells contained few peaks other than the peaks corresponding to elemental gold (Figure 2.10).

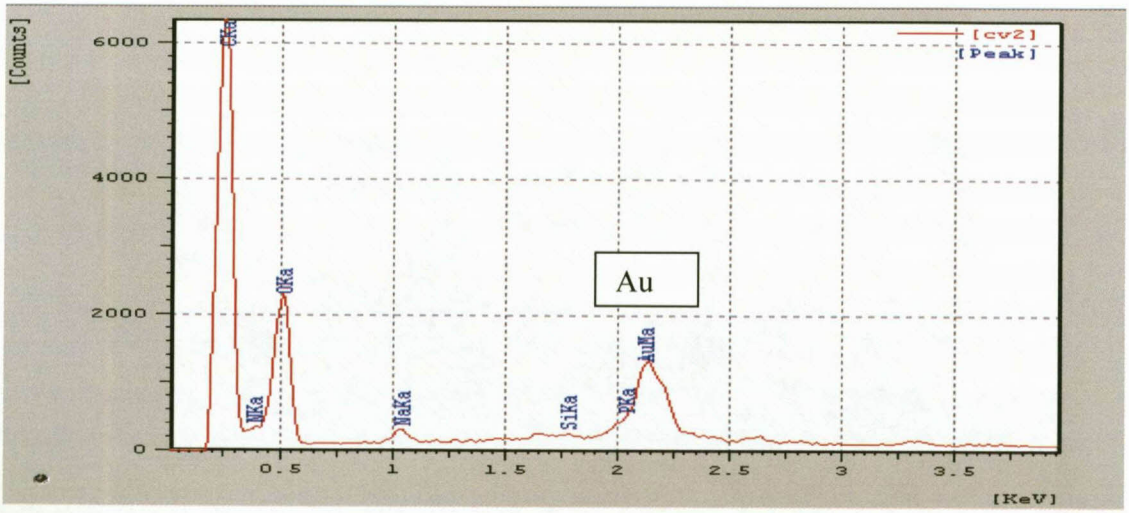

Figure 2.10: EDS spectra generated by *G. fermentans* biomass that was incubated with $HAuCl_4$, peak corresponding to elemental gold is marked with Au.

The high peak of carbon (Figure 2.10) has an effect on other elements' peaks. In that, the total percentage of carbon affects the total percentage of other detected elements, due to the semi-quantitative nature of the analysis. However, the presence of elemental gold was confirmed.

2.3.6 *Surface plasmon resonance band of Au nanoparticles formed by whole cells*

The gold nanoparticle formation can be monitored and analysed by the absorption of surface plasmon resonance band, which is characterized by maximum absorption at approximately 540 nm for particles with 50 nm diameter (Link and El-Sayed, 1999; Zhou *et al.*, 2001). In chapter 3 we will use this quantitatively to evaluate the nanoparticle formation.

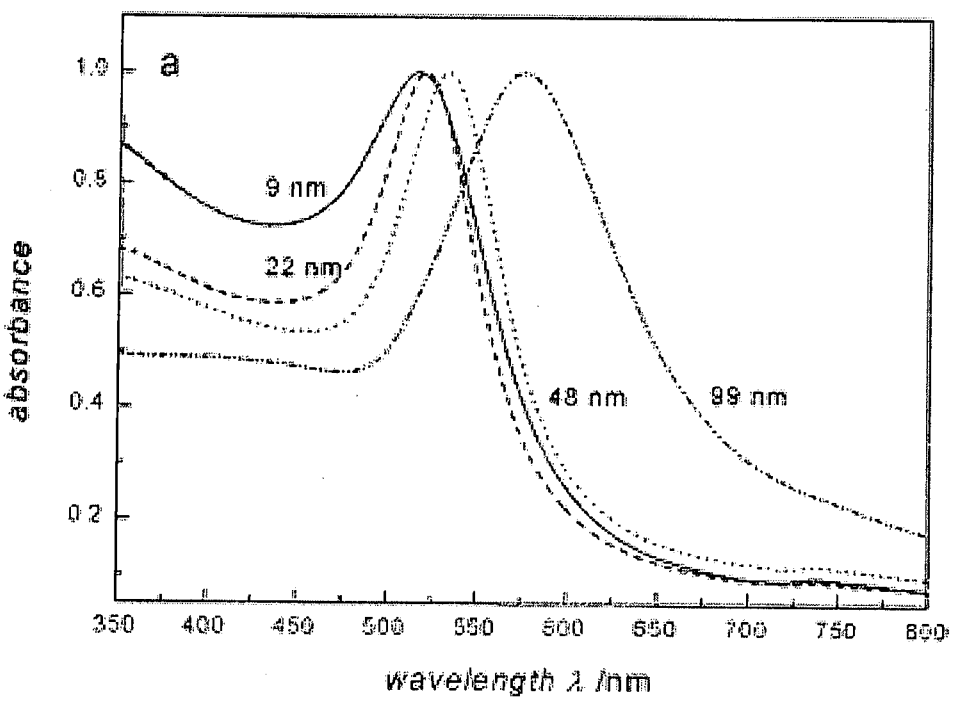

Figure 2.11: UV-Vis spectra for different sizes (9 nm – 99 nm) of gold nanoparticles (Taken from Link and El-Sayed, 1999).

Spherical gold nanoparticles with 9 nm diameters have a plasmon resonance band at 500 nm, an increase in particle size (mean diameter larger than 25 nm) shifts the plasmon resonance band to higher wavelengths (Figure 2.11).

The UV-Vis spectra recorded from whole cells that were incubated with 0.5 mM $HAuCl_4$ showed peaks that are characteristic of gold nanoparticles (Figure 2.12), with *G. fermentans* showing highest absorbance at 545 nm wavelength (Figure 2.12). The ability of whole cells to form nanoparticles intracellularly necessitates the use of cell free extracts for easier downstream processing.

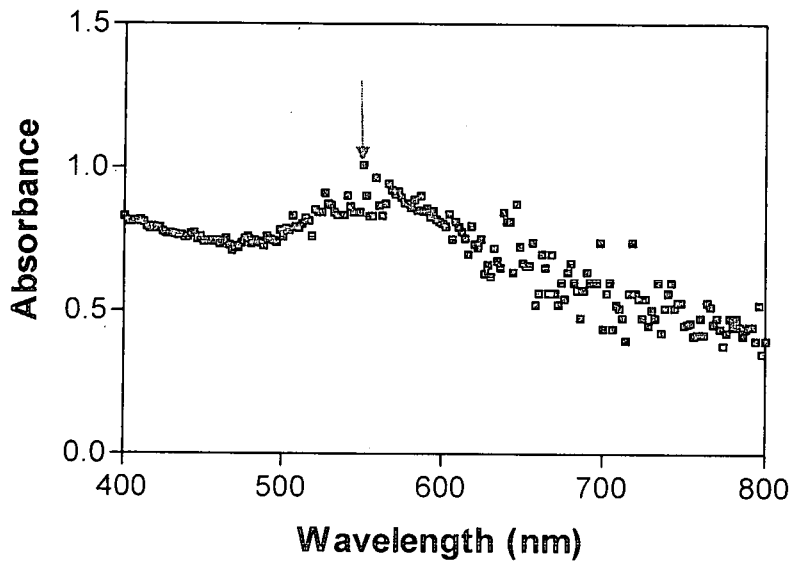

Figure 2.12: UV-Vis spectra for whole cells nanaoparicle formation by *G. fermentans*. The arrow points at the plasmon resonance band for Au nanopartice.

2.4 Conclusions

Various yeast species have the capability to interact with gold and form nanoparticles. *C. viswanathii, R. graminis and G. fermentans* had the most promising interactions with gold with respect to time and concentration of gold. *G. fermentans* is the best colloidal gold producer as evaluated under different gold ion concentrations and growth phase related ion removal. Nanoparticle formation was inhibited at 1mM $HAuCl_4$.

The TEM and UV-Vis spectra confirm the presence of gold nanoparticles in whole cells. Change of physicochemical parameters can influence nanoparticle formation as observe in the time dependent colour change of gold nanoparticle solution.

2.5 References

Ahmad, A., Mukherjee P., Senapati S., Mandal D., Khan I. M., Kumar R. and Sastry, M. 2002. Enzyme mediated extracellular synthesis of CdS nanoparticles by fungus, *Fusarium oxysorum*. *Journal of American Chemistry Society.*, **124:** 12108 – 12109

Ahmad, A., Mukherjee P., Senapati S., Mandal D., Khan I. M., Kumar R. and Sastry, M. 2003a. Extracellular biosynthesis of silver nanoparticles using the fungus *Fusarium oxysporum*. *Colloids and surfaces B: Biointerfaces.*, **28:** 313 – 318

Ahmad, A., Senapati, S., Khan M. I., Kumar, R., Ramani, R., Srinivas V. and Sasstry. M. 2003b. Intracellular synthesis of gold nanoparticles by a novel alkalotolerant actinomycete, *Rhodococcus* species. *Nanotechnology.*, **14:** 82 – 4828

Avery, S.V. and Tobin, J.M. 1992. Mechanisms of strontium uptake by laboratory and brewing strains of *Saccharomyces cerevisiae*. *Applied and Environmental Microbiology.*, **58:** 3883 – 3889

Beveridge, T.J. and Murray, R.G.E. 1976. Uptake and retention of metals by cell walls of *Bacillus subtilis*. *Journal of Bacteriology.*, **127:** 1502 – 1518

Brady, D. and Duncan, J.R. 1994. Bioaccumulation of metal cations by *Saccharomyces cerevisiae*. *Applied and Environmental Microbiology.*, **41:** 149 – 154

de Hoog, G.S., Smith, M.T. and Guého, E. 1998. *Geotrichum* Link: Fries. pp, 574 – 579. In: Kurtzman, C.P. and Fell, J.W. (eds). The yeasts, a taxonomic study. Elsiver, New York.

de Rome, L and Gadd, G.M. 1987. Measurement of copper uptake in *Saccharomyces cerevisiae* using a Cu^{2+}-selective electrode. *Federation of European Microbiological Societies Microbiology Letters.*, **43:** 283 – 287

Fell, J.W. and Statzell-Tallman, A. 1998. *Rhodotorula* F.C Harrison. Pp, 800 – 827. In: Kurtzman, C.P. and Fell, J.W. (eds). The yeasts, a taxonomic study. Elsiver, New York

Fujita, Y., Mori, I. and Matsuo, T. 1999. Spectrophotometric determination of gold(III) by an association complex formation between gold-thiamine and phloxine. *Analytical Sciences.* **15:** 1009 – 1012

Gadd, G.M. and Sayer, J.A. 2000. Influence of fungi and environmental mobility of metals and metalloids. Influence of Fungi on the Environmental mobility of Metals and Metalloids. pp, 237 – 256. *In*: Lovely D.R (ed). Environmental Microbe-metal interactions, *American Society for Microbiology Press*, Washington, D. C

Gericke, M. and Pinches, A. 2006. Biological synthesis of metal nanoparticles. *Hydrometallurgy.*, **83:** 132 – 140

Ibrahim, Z., Ahmad, W. A. and Baba, A.B. 2001. Bioaccumulation of silver and isolation of metal binding protein from *P. diminuta*. *Brazilian Archives Biology and Technology.*, 44: 223 – 225

Korobushkina, E.D., Biryuzova, V.I., Korobushkin, L.M. and Karavaiko, G.I. 1989. Origin and accumulation of gold crystals in yeast cells. *Proceedings of Academy of Science of United Soviet Socialist Republic.*, **304:** 431 – 433

Kowshik, M., Vogel, W., Urban, J., Kulkami, S.K. and Paknikar, K.M. 2002a. Microbial synthesis of semiconductor PbS nanocrystallites. *Advance Material.*, **14:** 815 – 818

Kowshik, M., Deshmukh, N., Vogel, W., Urban, J., Kulkami, S.K. and Paknikar, K.M. 2002b. Microbial synthesis of semiconductor CdS nanoparticles, their characterization, and their use in the fabrication of an ideal diode. *Biotechnology and Bioengineering.*, **78**: 583 – 588

Kowshik, M., Ashtautre, S., Kharrazi, S., Vogel, W., Urban, J., Kulkami, S.K. and Paknikar, K.M. 2003. Extracellular synthesis of silver nanoparticles by a silver-tolerant yeast strain MKY. *Nanotechnology.*, **14**: 95 – 100

Lengke, M. and Southam, G. 2006. Bioaccumulation of gold by sulfate-reducing bacteria cultured in the presence of gold(I)-thiosulfate complex. *Geochimica et Cosmochimica Acta.*, **70**: 3646 – 3661

Link, S. and El-Sayed, M.A. 1999. Size and temperature dependance of the plasmon absorption of colloidal gold nanoparticles. *Journal of Physical Chemistry B.*, **103:** 4212 – 4217

Lowenstam, H.A. and Weiner S. 1989. Biomineralization. Oxford University Press, New York Mann S, Webb J. and Williams, R.J.P (Eds), 1989. Biomineralization: *Chemical and Biochemical Persperctives*,325 pp, VCH Publishers, New York.

Melwanki, B., Masti, P, and Seetharamappa, J. 2002. Determination of trace amounts of gold(III) using Ethopropazine Hydrochloride and Idothipendyl Hydrocloride: A spectrophotometric study. *Turk Journal of Chemistry.*, **26:** 17 – 22

Mowll, J.L and Gadd, G.M. 1984. Cadmium uptake *by Aureobasidium pullulans. Journal of General Microbiology.*, **130:** 279 – 284

Mukherjee, P., Ahamad, A., Manda, D. Senapati, S., Sainkar, R.S., Khan, M.I., Ramani, R., Paricha, R., Ajayakumar, P.V, Alam, M., Sastry, M. and Kumar, R. 2001a. Fungus mediated synthesis of silver nanoparticles and their immobilization in the mycelial matrix: a novel biological approach to nanoparticle synthesis. *Nanotechnology Letter.*, **1:** 515 – 519

Mukherjee, P., Ahamad, A., Manda, D. Senapati, S., Sainkar, R.S., Khan, M.I., Ramani, R., Paricha, R., Ajayakumar, P.V, Alam, M., Sastry, M. and Kumar, R. 2001b. Bioreduction of $AuCl^-_4$ ions by fungus Verticillium sp. and surface trapping of the gold nanoparticles formed. *Angewandte Chemie International Edition.*, **40:** 3585 – 3588

Nair, B. and Pradeep, T. 2002. Coalescence of nanoparticles and formation of submicron crystallites assisted by *Lactobacillus* strains. *Crystal Growth and Design.*, **2:** 293 – 298

Raveendran, P., Fu, J. and Wallen, S.L. 2005. Completely "Green" synthesis and stabilization of metal nanoparticles. *Journal of American Chemistry Society.*, **125:** 13940 – 13941

Reese, R.N. and Winge, D.R. 1988. Sulfide stabilization of the cadmium-γ-glutamyl peptide complex of *Schizosaccharomyces pombe. Journal of Biology and Chemistry.*, **263:** 12832 – 12835

Sadler, P. 1976. The biological chemistry of gold: a metallodrug and heavy-atom label with variable valency. *Structure and Bonding.*, **29:** 171 – 213

Silver, S. 1996. Bacterial resistance to toxic metal ions - a review. *Gene.*,**179**: 9 – 19

Slocik, J.M., Stone, M.O. and Naik, R.R. 2005. Synthesis of Gold Nanoparticles using multifunctional peptides. *Small.*, **11**: 1048 – 1052

Senapati, S., Ahmad, A., Khan, M.I., Sastry, M. and Kumar, R. 2005. Extracellular biosynthesis of bimetallic Au-Ag alloy nanoparticles. *Small.*, **1**: 517 – 520

Southam, G and Beveridge, T.J. 1994. The in vitro formation of placer gold by bacteria. *Geochimica et Cosmochimica Acta.*, **58**: 4527 – 4530

Southam, G., Fyfe, W.S., and Beveridge, T.J. 2000. Immobilization of free ionic gold and L-asparagine-complexed gold by *Sporosarcina ureae*: the importance of organo-gold complexes in gold mobility. *Proceedings of Mining and Metallurgy.*, **17**: 129132

Sweeney, R.Y., Mao, C., Gao, X., Burt, J.L., Belcher, A.M., Geogiou, G. and Iverson, B.L. 2004. Bacterial biosynthesis of cadmium sulfide nanocrystals. *Chemistry and Biology.*, **11**: 1553 – 1559

Tobin, J.M; Cooper, D.J and Neufeld, R.J. 1984. Uptake of metal ionsby *Rhizopus arrhizus* biomass. *Applied and Environmental Microbiology.*, **47**: 821 – 824

Van Wyk, P.W.J. and Wingfield, M.J. 1991. Ascospores ultrastructure and development in *Ophiostoma cullulatum*. *Mycologia.*, **83**: 698 – 707

White, C and Gadd, G.M. 1987. The uptake and cellular distribution of zinc in *Saccharomyces cerevisiae*. *Journal of General Microbiology.*, **133**: 727 – 737

Zhou, Y ., Itoh, H., Uemura, T ., Naka, K. and Chujo, Y. 2001. Preparation of p-conjugated polymer-protected gold nanoparticles in stable colloidal form. *Chemical Communications.*, **7:** 613 – 614

Chapter 3

In vitro synthesis of gold nanoparticles, identification and characterisation of involved enzyme(s)

3.1 Introduction

Biological systems are complex, with synthesis, structure and function rarely understood in detail. Furthermore, biological systems are used to "build" nanoparticles of specific morphology and function (Eustis and El-Sayed, 2005). The difficulty in synthesizing nanoparticles of the desired size, shape and monodispersity directs research into new and redefined synthetic methods. Generation of the desired chemical and physical interfaces to interact with target molecules also require the need for many different synthetic methods for nanoparticle synthesis (Eustis and El-Sayed, 2005). The electrostatic and topographic properties of biological macromolecules and their derived supramolecular complexes can be used for the synthesis and assembly of inorganic particles (Niemeyer, 2001). Horse spleen apoferritin was used as a template for synthesis of manganese oxide and uranyl oxyhydroxide nanoparticles, by basic hydrolytic polymerization of uranyl acetate, leading to the formation of uniform 6 nm within the spatially confined protein cage (Meldrum *et al.*, 1991). The use of protein molecules for nanoparticle synthesis is interesting, in that structures can be rationally designed on the same size as biological molecules that act as templates. Thus, generating the ability to probe and modify biological systems. Cavities formed by proteins have occasionally been used as reaction chambers for the synthesis of nanoparticles (Yoshimura, 2006).

With the use of microorganisms for nanoparticle synthesis, the mechanism with which this synthesis occurs is not yet elucidated and neither has the enzymes involved been characterized. However, recently it has been reported that NADH dependent enzymes in an electron system shuttle may be responsible for bioreduction of Au^{3+} to Au^{0} and the resulting nanoparticle formation (He *et al.*, 2007). Duran *et al.*, (2005) suggested that extracellular synthesis of silver

nanoparticle in *F. oxysporum* result from a process that probably involves either a reductase action or by electron shuttle quinones or both. Shivshankar *et al.* 2004 reported that the formation of pure metallic nanoparticles and bimetallic nanoparticles by reduction of the metal ions is possibly facilitated by reducing sugars and/or terpenoids present in the neem leaf broth.

This chapter seeks to, (i) identify and characterize the main protein(s) involved in gold reduction that is associated with nanoparticle formation and (ii) characterize the nanoparticles in these reaction systems.

3.2 Materials and methods

3.2.1 *Cell fractionations*

Cells were grown and harvested as described in section 2.2.1. Wet biomass was resuspended in acetate buffer (0.1M, pH 5.0), ratio of biomass to beads (200 mg : 1.0 g) in 1 ml final volume. The suspension was vortexed for 1 min and cooled for 1 minute, with cell burst time of 20 minutes. The extent of disruption was monitored under light microscope. Cell debris was removed by centrifugation (10 000 *x g*, 10 min, 4°C), the supernatant was kept and pellet discarded. Separation of cytoplasmic and membrane proteins was done by ultracentrifugation (100 000 x g, 1.5 hours, 4°C), (method adapted from Mitt *et al.* 1990). The use of glass beads for breaking cells replaced the use lyticase for breaking cells which was used in the original method. All fractions were assayed for nanoparticle formation activity as described in section 2.2.2 and/or 2.3.4.

3.2.2 *Protein assay*

Protein concentrations were estimated by absorbance at 280 nm (column elutes) or by using the bicinchoninic acid (BCA) method (Smith *et al.,* 1985) according to manufactures guidelines, Pierce (Rockford, IL, USA). The standard protein assay was used. The method of the assay was supplied with the commercially available kit. A set of protein standards was prepared with bovine serum albumin (BSA), provided by Pierce as part of the BCA protein assay kit in the range of 0-2000 μg/ml. The standard curve was prepared and used to determine the protein concentration of unknown protein samples.

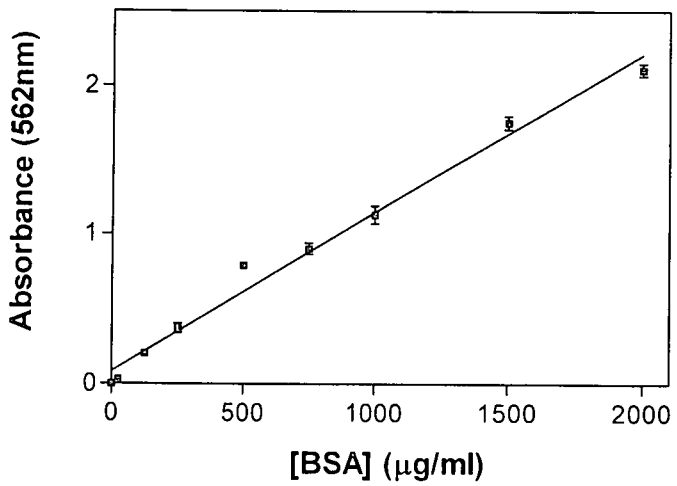

Figure 3.1: Standard curve for the protein concentration using the BCA assay. Error bars indicate standard deviation.

3.2.3 *Evaluation of nanoparticle formation under various physico-chemical conditions*

The protein extracts were prepared as described in section 3.2.1, however the extract were used before subcellular fractionation. Protein concentrations were determined using BCA assay kit as described in section 3.2.2. The standard protein concentration used for cell free extracts was 40 µg/ml, the reaction mixture contained protein dissolved in acetate buffer (pH 5.0) and $HAuCl_4$.

Temperature, pH and gold ion concentrations were varied with standardised cell-free extracts. The formation of gold nanoparticles was followed by the visual assay (Section 2.2.2).

The effect of temperature was evaluated on three gold ion concentrations i.e. 0.1 mM, 0.5 mM and 1 mM. The effect of pH was also evaluated under the three mentioned gold ion concentrations at 25°C over 12 hours time period. Acetate buffer was used for pH 3 and 5, while phosphate buffer was used for pH 7.9 and CAPS for pH 11.

3.2.4 *Characterization of in vitro synthesized gold nanoparticles*

3.2.4.1 *UV-Vis spectral analysis*

The visual assay was used as in section 2.2.2 to follow gold nanoparticle formation; however it was complemented by evaluation of the plasmon resonance band (Section 2.3.4).

The UV-Vis spectroscopy measurements of the gold nanoparticle containing solutions were made on a UV-Visible spectrophotometer (Beckman Coulter, model DU 800), operated in an absorbance mode with scan speed of 1200 nm/min.

3.2.4.2 *TEM and EDS analysis*

The films of gold nanoparticles were prepared on carbon coated copper grids by drop-coating with nanoparticle solution, followed by evaporation at room temperature. TEM and EDS analysis were performed on Joel 6400 WINSEM (Japan) and a Philips CM 100 (The Netherlands).

3.2.5 *Substrate specificity*

3.2.5.1 *Nitrate reductase assay*

Nitrate reductase activity was assayed by measurement of nitrite formation using a modified method of Showe and DeMoss (1968). The assay was carried out in eppendorf tubes containing in a final volume of 1ml: Na_2NO_3, (20 μmoles), potassium phosphate buffer, pH 7.7, (20 mmoles), methyl viologen, (0.1μmoles), Na_2HCO_3, (9.5 μmoles), $Na_2S_2O_4$, (4.6 μmoles), and cell extract protein, (20 μg), depending on the protein content of the extract. The reaction was started by addition of a freshly prepared solution of $Na_2S_2O_4$ in Na_2HCO_3. Before

incubation, the reaction was flushed with CO to displace O_2 and incubation was at 30°C for 10 min. The reaction was ended by vigorous shaking, which oxidized the remaining dithionite. To determine **nitrite**, two parts of 4% (w/v) sulphanilamide and 25% (v/v) HCl solution were mixed with one part of 0.08% (w/v) *N-1*-napthhylethylene-diamine dihydrochloride, 0.3 ml of this mixture was added to 1ml of the nitrite containing sample. After 10 min, the absorbance of the mixture was read in a spectrophotometer at 540 nm wavelength.

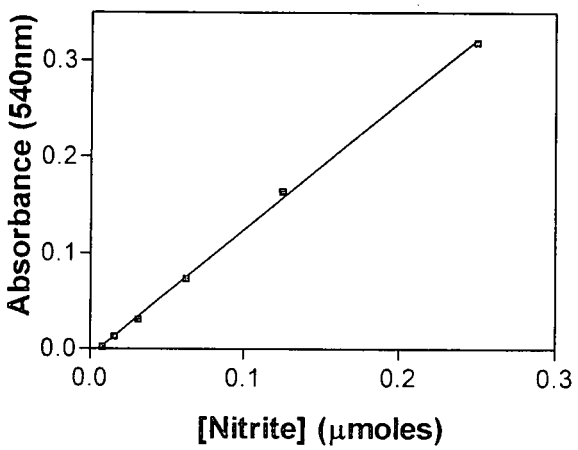

Figure 3.2: A standard curve for nitrate reduction assay. Duplicate determinations were done and the variations were smaller than the symbols used for the data points.

Definition of enzyme units and specific activities: One unit of enzyme is defined as the amount of enzyme that will transform one μmole of nitrate to nitrite in 10 min. Specific activity is defined as enzyme units per microgram of protein.

3.2.5.2 *Fe^{+3} reductase assay*

A continuous assay was used to monitor the enzyme catalyzed reduction of Fe^{+3} to Fe^{2+}. The reaction contained HEPES, pH 7.7, 50 mM, ferrozine, 1 mM, Fe(III)-NTA (nitriloacetic acid), 2 mM and NADH, 1 mM. The absorbance was measured at 562 nm with a Beckman Coulter DU 800 (Under aerobic conditions)

(Stookey, 1970). The used standard curves were obtained from an M.Sc thesis by Bester, 2007.

3.2.6 *Column chromatography*

Small scale columns were used to evaluate the different resins available in our laboratory for purification, the spectrum covered cation exchange, anion exchange and hydrophobic interaction columns. Protein extract (500 µg/ml) was allowed to interact with these resins. The proteins eluted and both the binding and non-binding fractions assayed for activity. The Super Q resin from Tosoh was the most efficient in binding, since the protein that showed nanoparticle formation was retained on this resin.

3.2.6.1 *First purification attempt*

The cytoplasmic protein fraction was obtained as described in section 3.2.1. Cytoplasmic fraction was applied to Super Q (120 X 25 mm) anion exchange column, equilibrated with 20 mM Phosphate buffer (pH 7.7). The enzyme was eluted with increasing salt gradient (0-1 M NaCl (500 ml)) at a flow rate of 5 ml/min. Salt concentration was determined by conductivity measurements. Fractions (10 ml) were collected, the absorbance monitored at 280 nm and assayed for activity. Those fractions containing bulk of activity were pooled.

A fraction of contaminating proteins showed no interaction with the resin and eluted before the start of the salt gradient. SDS PAGE was used to evaluate the homogeneity of the fractions.

3.2.6.2. *Second purification attempt*

The same protocol as described in section 3.2.6.1 was followed, the pooled protein fraction was reloaded on the Super Q column under the same column

conditions and the active fraction eluted a second time. A loss of activity was observed after the second column step.

3.2.6.3 *Third purification attempt*

The crude extract was loaded onto a secondary Super Q column, equilibrated as described in section 3.2.6.1. The proteins were eluted and evaluated for nanoparticle formation activity. The eluted proteins were dialysed extensively against 20 mM phosphate buffer to remove the salt, then loaded into Sephacryl S-300 column that was equilibrated with 20 mM phosphate buffer (pH 7.7). Fractions (2 ml) were collected, the absorbance monitored at 280 nm and assayed for activity. The collected fractions were assayed for nanoparticle formation activity by monitoring the plasmon resonance band. Nanoparticle formation activity was lost again and therefore the purification in section 3.2.6.2 was the preferred strategy, with the possible addition of NADH or other electron donors to restore nanoparticle formation activity.

3.2.7 *Identity confirmation of the studied yeast*

Cells were grown for 48 hours at 25°C in 50 ml Erlenmeyer flask with YM broth. DNA was extracted as described by Labuschagne and Albertyn, 2001. The divergent D1/D2 domain (nucleotides 63-642 for *Saccharomyces cerevisiae)* at the end of the large sub-unit (LSU) rRNA gene was symmetrically amplified with primers NL-1 (5'-GCATATCAATAAGCGAGGAAAAG) and NL-4 (5'-GGTCCGTGTTTCAAGACGG) (O'Donnel, 1993).

A PCR was performed on the isolated genomic DNA from *G. fermentans* to amplyfy the divergent D1/D2 domain. The PCR mixture contained 2 µl (100ng) of isolated genomic DNA, 1.25 µl of each of the primers (80 x 10^{-12} mol/µl), 1 µl of dNTP's (10 mM), 0,25 µl of Taq DNA Polymerase(5 units), 0.5 µl of 10x *Taq* DNA Polymerase buffer, 1 µl of BSA (10µg/ul) and 16.25 µl distilled water. The

reaction was set with the initial denaturation of the template at 94°C for 2 minutes followed by 36 cycles of denaturation at 94°C for 60 seconds, annealing at 52°C and elongation at 72°C for 2 minutes. Visualization of the extracted and amplified DNA was performed following electrophoresis in 1 % agarose in 1 X TAE buffer (0.04 M Tris-acetate, 0.001 M EDTA [pH 8.0] and staining with ethidium bromide (8×10^{-5} µg/ µl). Sequencing of the PCR product was done at Inqaba Biotechnology (Pretoria, South Africa) using an ABI V3.1 Big dye kit and precipitated with the Zymo Research Sequencing clean-up kit.

3.3 Results and discussion

3.3.1 *Effects of physico-chemical factors on nanoparticle formation*

Table 3.1. Evaluation of nanoparticle formation by cell-free extracts at different temperatures (pH 5).

Au^{3+} Conc. (mM)	Organism	15°C	25°C	37°C *	42°C *	65°C
0.1	*C. viswanathii*	-	+	+	++	++
	G. fermentans	-	+	++	+++	+++
	R. graminis	-	++	++	++	+++
0.5	*C. viswanathii*	-	+	+++	+++	+++
	G. fermentans	+	+++	+++	+++	+++
	R. graminis	+	+++	+++	+++	++++
1.0	*C. viswanathii*	-	+	+++	++++	++++
	G. fermentans	+	++++	++++	++++	++++
	R. graminis	+	++++	++++	++++	++++

* indicates best working temperature range

The optimum growth temperature for yeast species is around 25°C (de Hoog *et al.,* 1998; Fell and Statzell-Tallman, 1998; Meyer *et al.,* 1998), however, even though nanoparticle formation occurred at this temperature, one could significantly increase nanoparticle formation by increasing temperature. Thermodynamically this was most likely to proceed faster as one would expect with protein catalyst. Blank rates however did not change significantly, Results of independent studies showed gold nanoparticles forming at higher temperatures to be bigger and amorphous (section 2.3.3). The initial concentration of $HAuCl_4$ ions can influence nanoparticle formation, at low concentration and low temperature nanoparticle formation was not observed, however an increase in $HAuCl_4$ concentration resulted in nanoparticle formation (Table 3.1. These concerted effects of two factors were also observed in Table 3.2, with pH and gold ion concentration varied. Acidic and alkaline pH decreased

nanoparticle formation, however, pH 5 and 7 were optimal for nanoparticle formation.). It was observed that nanoparticles formed at 1 mM $HAuCl_4$, contrary to what was observed with whole cells experiments in the same $HAuCl_4$ concentration.

Table 3.2. Evaluation of nanoparticle formation by cell-free extracts at different pH conditions (42°C)

$HAuCl_4$ Conc. (mM)	Organism	pH 3	pH 5	pH 7	pH 9	pH 11
0.1	*C. viswanathii*	-	-	-	-	-
	G. fermentans	-	++	+	-	+
	R. graminis	-	+	++	-	+++
0.5	*C. viswanathii*	-	+++	+++	+++	-
	G. fermentans	-	+++	++	++++	+
	R. graminis	-	++++	+++	+++	++
1.0	*C. viswanathii*	++++	++++	++++	-	++
	G. fermentans	++++	+++	++++	++	++
	R. graminis	++++	++++	++++	+++	++

3.3.2 *Subcellular fractionation*

Cytoplasmic and membrane proteins were isolated as described in section 2.2.4, the ability of each of these fractions were evaluated for gold nanoparticle formation activity (Figure 3.3).

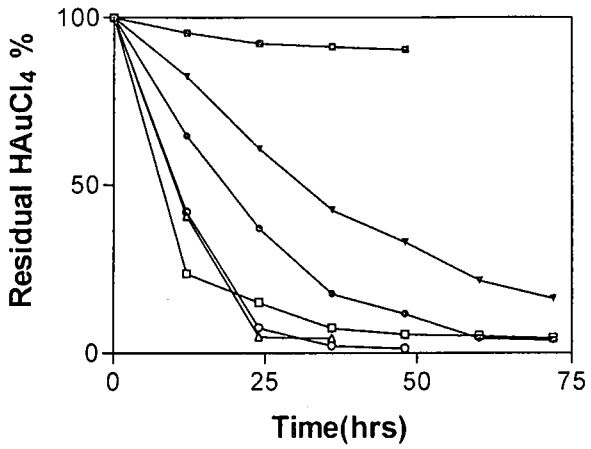

Figure 3.3: Percentage $HAuCl_4$ removal by cell free extracts, *C.viswanathii* (•), *G. fermentans* (▼) and *R. graminis*(▪), open symbols represents cytoplasm and solid symbols represent membrane fractions. Residua $HAuCl_4$ concentations were determined using the phloxine assay, average of triplicate values was used for the graph.

Gold nanoparticle formation activity, which usually indicates reduction was higher in cytoplasmic fractions than in membrane fractions. The membrane fraction of *R. graminis* showed no reducing activity. The fractions of *G. fermentans* exhibited a clear difference in visual analysis, for nanoparticle formation, this was indicative of possible different size or morphology of the nanoparticles formed. The blue colour seen in nanoparticle formed by cytoplasmic fraction of *G. fermentans* attracted more attention and future research was done on this cytoplasmic fraction.

3.3.3 *Surface plasmon of gold nanoparticles formed by cytoplasmic fraction*

The ultraviolet-visible spectra of cytoplasm fraction incubated with 0.5 mM Au^{3+} gold ions for 12 hours showed maximum absorbance at 545 nm which is characteristic of gold nanoparticles and the solution turned purple. A slightly blue colour was observed for the cytoplasmic fraction of *G. fermentans,* when incubation time was extended to 24 hours. The blue colour formation resulted in broadening of the plasmon resonance band as well as a slight shift to a higher

wavelength for maximum absorption (Figure 3.4), which usually indicate an increase in size of the formed nanoparticles. This is an important parameter to consider in custom made nanoparticles.

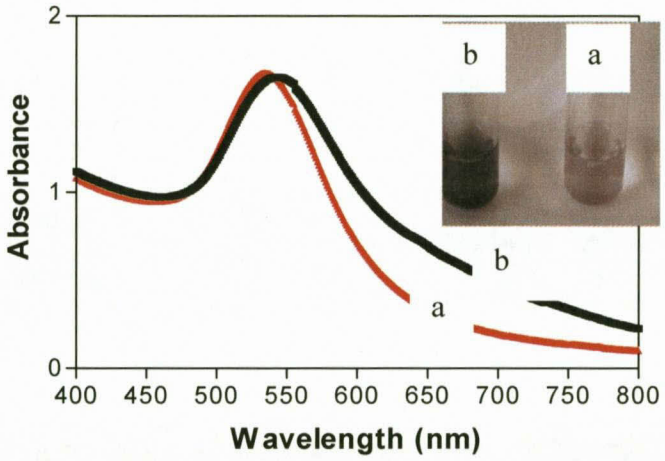

Figure 3.4: UV-Vis spectra of the cytoplasmic fraction of *G.fermentans* incubated for 12 hours (a) and 24 hours (b). The insert is a picture illustrating the respective gold nanoparticle containing solutions.

The ability of cell free extract to form gold nanoparticles was encouraging, given that both whole cells and cell free extract gold nanoparticle solutions absorbed maximally at 545 nm, thus suggesting that nanoparticles formed in both solutions were of the same size distribution. Nanoparticles of the same size have the same maximum absorption wavelength (Link and Al-Sayed, 1999). The time dependent shift of LSPR to higher wavelengths observed in gold nanoparticle solution of *G. fermentans'* cytoplasmic fraction indicates agglomeration or an increase in size of nanoparticles in solution (Aslan *et al.,* 2005). A lack of nanoparticle agglomeration in all membrane fraction solutions was observed. A crude extract of cytoplasmic proteins is naturally expected to have an abundance of reducing agents e.g. sugars, NADH and other organic acids. Two scenarios can explain the observed agglomeration. One, nanoparicles formed by a chemical process will easily agglomerate due to a lack of capping agent, capping agents are used to stabilized nanoparticles when chemical synthesis methods

are used (Raveendran *et al.,* 2003). Two, capping molecules can result in a shift of the plasmon absorption peak (Aslan *et al.,* 2005). When the cell free extract was denatured by heat, no nanoparticle formation was observed (data not shown). Thus, this study achieves to demonstrate the first aim: proteins/enzymes are responsible for gold nanoparticle formation. In this regard, proteins can facilitate reduction and simultaneously act as a capping agent or provide a nucleation site for nanoparticle formation (Slocik *et al.* 2005). For nanoparticle synthesis to occur, a reducing agent and a nucleation site are required (Carrot *et al.*, 1998).

3.3.4 *Partial purification of protein involved in nanoparticle formation*

A purification of the nanoparticle forming enzyme was done on anion exchange column. The first purification attempt of Super Q column yielded a protein peak that showed reducing ability and nanoparticle formation, several contaminating proteins separated from this fraction.

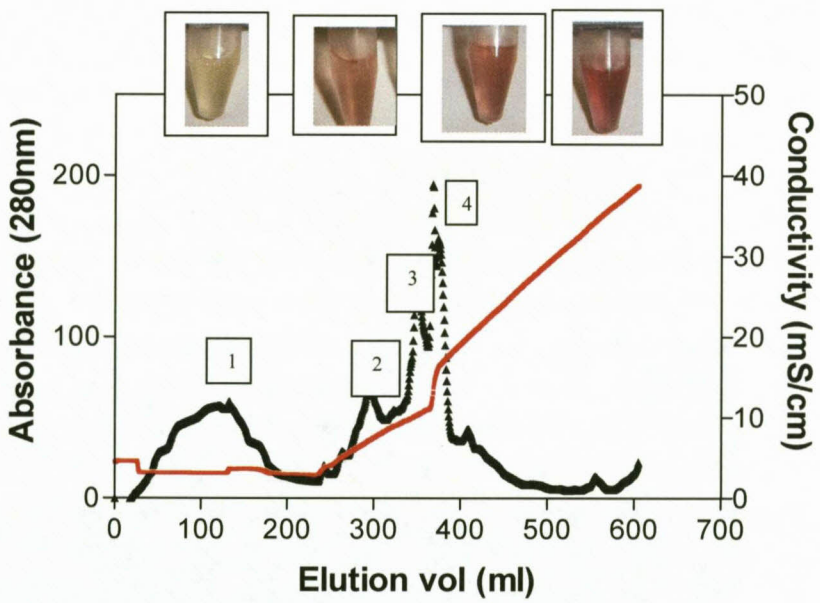

Figure 3.5: Primary column elution profile of cytoplasmic proteins. Labelled peaks were assayed for nanoparticle forming activity. The secondary axis indicates an increasing salt gradient. The insert is a picture of the respective fractions' visual analysis in order of nanoparticle colours.

A second anion exchange step was done to further remove contaminating proteins (Figure 3.6). The protein fractions were incubated with gold ions and nanoparticle formation was observed. However, this purification step was accompanied by a loss in nanoparticle formation activity.

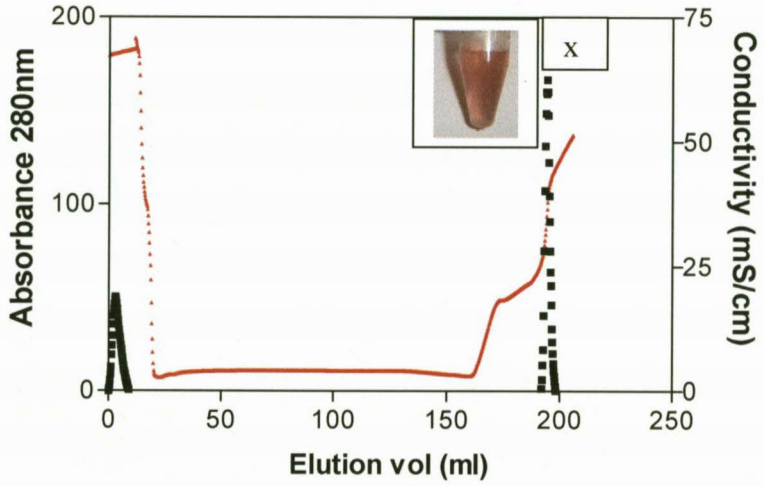

Figure 3.6: Secondary column elution profile of cytoplasmic proteins. X indicates the nanoparticle forming fraction and the visual assay of the nanoparticle is displayed. The secondary axis indicates an increasing salt gradient.

Purification attempts other than the first one led to a loss in nanoparticle formation ability, possibly indicative of the stripping of necessary elements or unfolding for this "reductase" or fortuitive protein action on the gold particle formation.

Attempts were made to enhance the activity as suggested by Anil *et al.* 2007. The protein was also incubated with 1.5 mM NADH as a cofactor. The activity improved and nanoparticle formation was evaluated. The stochiometry of Au^{3+} to NADH was calculated based on the number of electrons required to reduce 0.5 mM Au^{3+} completely. Table 3.3 summarises the purification procedure as described in section 3.2.6.2 of isolating a nanoparticle forming protein.

Table 3.3 Purification table for the purification protocol of yeast gold nanoparticle forming protein

Fraction	Volume (ml)	Conc. (ug/ml)	Total protein (mg)	Activity* (nmoles/ minl)	Total units (U)	%Yield protein	%Yield Activity	Specific actitity (nmoles/ min.mg^{-1})	Purification factor
Crude	150	2265	340	0.92	0.137	100	100	0. 41	1.0
Primary SQ cytoplasmic fraction	10	502	5.02	0.17	0.002	1.47	18.4	0. 34	0.83
Secondary SQ cytoplasmic fraction	10	20	0.2	0.12	0.001	0.06	13.2	6.05	14.9

*One unit of enzyme activity is defined as the amount enzyme required to remove one mole of $HAuCl_4$ per minute from solution using Pholoxine assay. The protein was enriched 15 times.

SDS-PAGE analysis was used to evaluate the homogeneity of the active fractions. The second column step still yielded multiple bands on SDS PAGE analysis, with one intense band that is approximately 38 KDa in size.

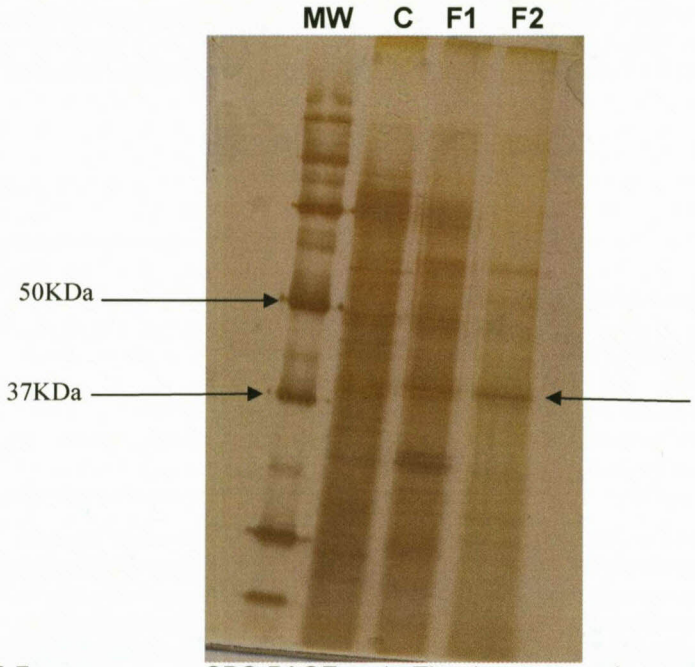

Figure 3.7: SDS-PAGE gel. The lanes contain protein molecular weight marker (MW), crude fraction (C), active fraction from primary column (F1) and active fraction from secondary column (F2). The arrow in lane F2 points to the band of interest.

In order to try to restore or enhance the activity different co-factors were evaluated for their ability to restore the nanoparticle forming activity of the

purified sample. He *et al.* 2007 reported that gold nanoparticle formation is due to NADH and NADH-dependent enzymes in gold nanoparticle synthesis by microorganisms. Many authors report on the ability of enzymes to reduce metals using an electron shuttle systems in which a co-factor acts as an electron donor.

$FADH_2$ (0.75 mM) was unable to restore activity, while 1.5 mM NADH and 1.5 mM NADPH were effective. However, high blank rates were observed with NADPH and as a result, it was not the preferred co-factor in this study. Finally, gold reduction could be enhanced by 1.5 mM NADH.

3.3.5 *Substrate specificity evaluation*

It has become common for enzymes to catalyse reactions that are inconsistent with their metabolic function, especially in metal reduction. Anil *et al.*, 2007 reported a nitrate reductase–mediated synthesis of silver nanoparticles from $AgNO_3$ and Opperman and Van Heerden (2008) reported the dihydrolipoamide dehydrogenase from *Thermus scotoductus* able to reduce chromate.

Anil *et al.*, 2007 reported that the protein responsible for silver reduction may be a putative nitrate reductase. Barbier and Campbell, 2005 also described several other partial activities of nitrate reductase e.g dehydrogenase activity, NADH: ferricyanide reductase activity thus it is not inconceivable that gold may be another substrate option. This shows the versatility of the enzyme in substrate accommodation.

Table 3.4 summarises the purification procedure used in section 3.2.6.2 of isolating a nanoparticle forming protein, but the gold reduction assay was replaced with an assay for nitrate reductases as discussed in section 3.2.5.1.

Table 3.4. Purification table for the purification protocol for yeast nitrate reductase protein

Fraction	Volume (ml)	Conc. protein (ug/ml)	Total protein (mg)	Activity* (nmoles/ min/ml)	Total units (U)	%Yield protein	%Yield Activity	Specific activity (nmole/min.mg^{-1})	Purification factor
Crude	15	268	4.02	0.21	3.17	100	100	0.053	1.0
Primary SQ cytoplasmic fraction	10	226	2.06	0.22	2.20	51.2	69	0.107	2.02
Secondary SQ cytoplasmic fraction	10	40	0.4	0.44	4.41	9.95	139	1.10	20.7

*One unit of enzyme is defined as the amount of enzyme that will transform one μmole of nitrate to nitrite in 10 min. Specific activity is defined as enzyme units per microgram of protein.

A two fold purification of the nitrate reductase was observed in the primary column step, which is a better indication of isolation in comparison to Table 3.3. In secondary column step, a 20-fold purification of the enzyme was obtained with a specific activity of 1.10 U/mg. A loss of activity was observed in the primary column, however the secondary column step gave two fold increase in activity compared to the crude extract (Table 3.4). It is not common to gain activity during purification unless there was a removal of inhibitors or assay conditions were not optimised, in Table 3.4 the increase in activity could be ascribed to the addition of NADH in the last column step. The activity values as depicted in the purification Table 3.4 corroborate with the intensity of the marked band of interest on SDS-PAGE, thus suggesting an enrichment of the band in question (Figure 3.7 and Table 3.4). It was observed that the intensity of this band increases with each purification step. Reductase activity was observed in all three fractions that could form gold nanoparticles as shown in Figure 3.5 (Peaks 2, 3 and 4).

Minimum functional size of nitrate reductase in eukaryotic cells is 30 kDa and maximum functional size being 102 kDa (Barbier and Campbell, 2005), the huge difference in size is due to variable number of domains and/or complementing prosthetic groups at the redox centre. The size of the enriched band is within the reported range of nitrate reductases of eukaryotic origin. An attempt of removing

contaminating bands by gel filtration was not successful, since no distinct protein was eluted and activity was lost. It is not impossible for nitrate reductase to catalyse the reduction of $HAuCl_4$. The nitrate-binding site in nitrate reductase is surrounded by positively charged residues that create a cavity or substrate funnel, this is consistent with the binding of an anion substrate i.e. nitrate. However, a patch of negative charge lies immediately above the entrance to the substrate funnel (Eckardt, 2005), possibly the negatively charged patch allows Au^{3+} binding. Evaluation of other reduction activities indicated no significant alternative.

Relating activity to possible NADH dependant reductases and to explore the effect of NADH on specific activity the assay for iron reduction was attempted. But upon investigating the possible metal reductase activity of the final protein fraction, there was no increase of Fe(II) ion concentration over time for the duration of incubation period of 10 min. Therefore, we conclude that this is no ordinary iron reductase activity with a possible wide substrate specificity that will include Au^{3+} as alternative substrate.

3.3.6 *Nanoparticle characterization*

Characterizations were done according to discussed in sections 3.2.4.2, however additional methods will be described throughout the discussion. Also diffraction analysis was done as reported by Chah *et al.* 2002.

The partially purified protein fraction formed small gold nanoparticles (Figure 3.8) that were evenly distributed with occasional clustering, the average size of the nanoparticles was found to be 15 nm, the analysis was performed by (British Biocell International) under the supervision of Dr. Darren Knowles. It is well known colloidal paricles are inevitably spread in diameters, due to the fact that heterogeneous nucleation is thermodynamically much more favourable than the

homogeneous one to have (Sear, 2007). Figure 3.8 show a significant degree of monodispersity.

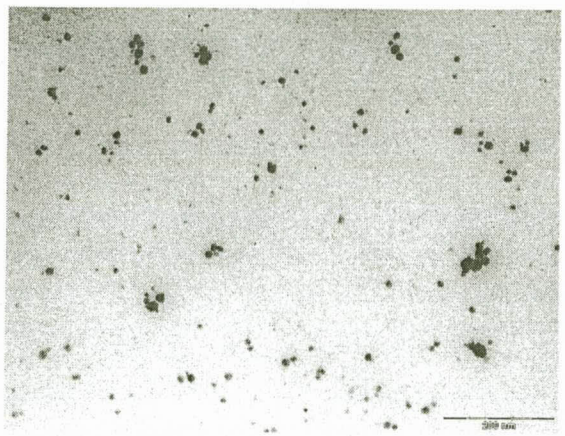

Figure 3.8: TEM micrograph of gold nanoparticles synthesised by the purified protein extract from the first column step. Scale bar is 200 nm.

It was observed that nanoparticles formed by protein extracts from the first column step were predominantly clustered (Figure 3.9). The clusters could be formed by non-specific capping by different proteins, also suggested by Aslan *et al.* 2005. It is essential for the capping agent to provide steric repulsion to avoid agglomeration of the formed nanoparticles (Niemeyer, 2001). A distinct or partially purified protein could provide that steric repulsion as opposed to a crude proteins extract.

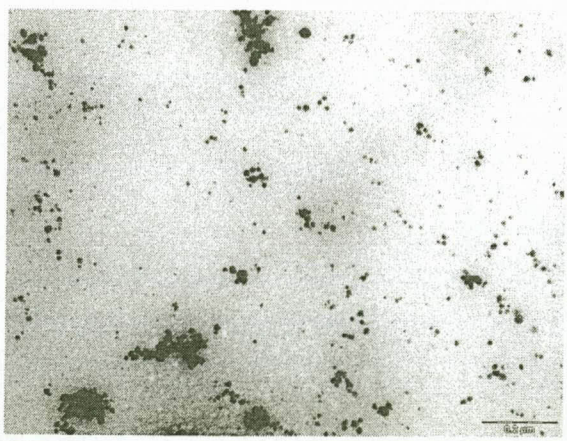

Figure 3.9: TEM micrograph of gold nanoparticles synthesised by the purified protein extract from second column step. Scale bar is 200 nm.

The analysis is done in a standard QC testing procedure, this comprises of two different operators measuring 50 particles of one grid (noting that each operator measures a different grid). The raw data for each set of 50 particles is then put into a spreadsheet and a mean size and percentage (size distribution) is determined from the analysis. The same is also done with the second operator's 50 particles and then both results are averaged and a final size and final percentage size distribution for a sample is calculated.

Electron diffraction patterns generated from these particles showed three rings in a hexagonal patter which indicates that the presence of octahedral gold , the electron diffraction pattern indicates the polycrystalline nature of the observed nanoparticles (Figure 3.10), a ring- type doted pattern is characteristic of polycrystalline material (Chah *et al.,* 2002), indicating that smaller nanoparticles formed aggregates. The accompanying EDS spectra confirmed the presence of only elemental gold in these particles (Figure 3.11).

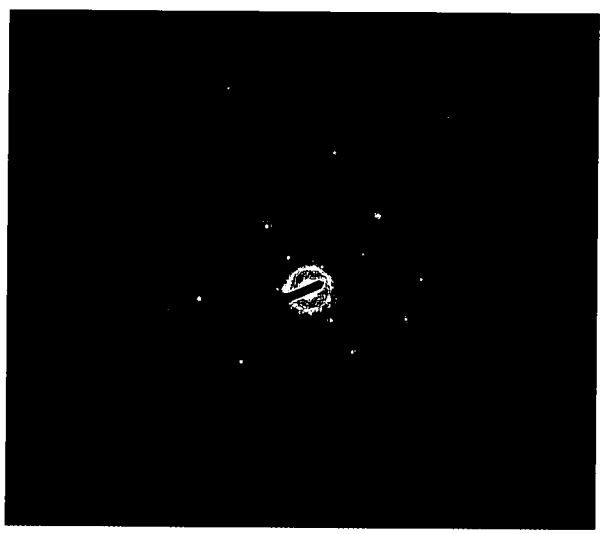

Figure 3.10: Diffraction pattern of gold nanoparticles formed by partially purified fraction.

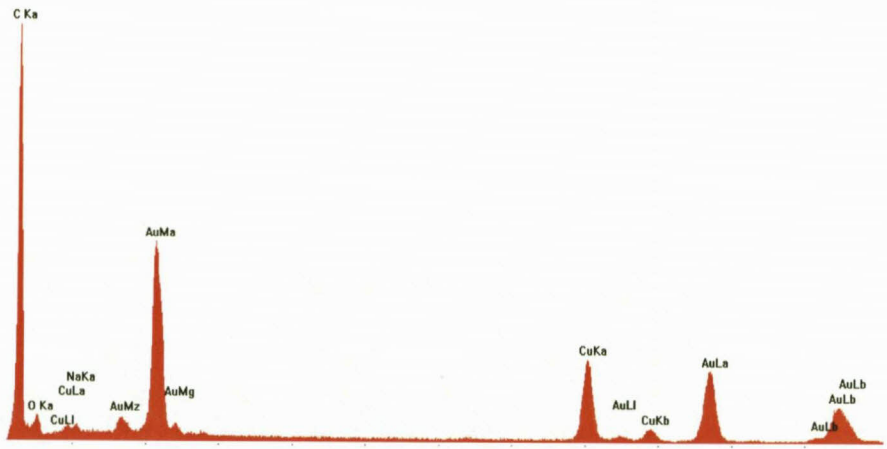

Figure 3.11: EDS spectra of gold nanoparticles formed by partially purified fraction

3.3.7 *Final confirmation of yeast species identity*

Identification of the yeast, *G. fermentas*, was confirmed by molecular characterization as described by Kurtzman and Robnette, 1998, although it was received from the UNESCO MIRCEN Yeast culture collection. Yeast identity had to be confirmed for final publications.

Yeast genomic DNA was isolated from the yeast of interest as described in section 3.2.7. Figure 3.12 depicts pure genomic DNA isolated from *G. fermentans*, a yield of 454 and 757 ng/μl was achieved, for lane 2 and 3 respectively.

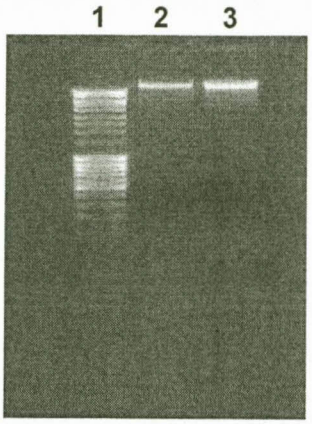

Figure 3.12: An ethidium bromide stained 1 % agarose gel showing the isolated yeastl genomic DNA. Lane 1, DNA marker, lane 2 and 3, genomic DNA isolated from *G. fermentans*.

3.3.8 *PCR amplification of the D1/D2 domain*

The divergent D1/D2 domain is at the 5' end of large sub-unit (LSU) rDNA gene of yeast is generally sufficient to resolve individual yeast species, the size of this gene is 600bp (Kurtzman and Robnett, 1998). Thus, used in this chapter for confirmation of *G. fermentans*. Figure 3.13 is an agarose gel showing a 600bp DNA fragment obtained after amplification of the D1/D2 domain of *G. fermentans*.

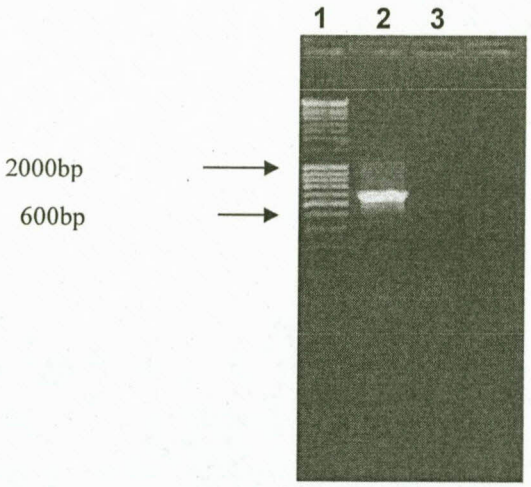

Figure 3.13: An ethidium bromide stained 1 % agarose gel showing PCR product. Lane 1, marker, lane 2, amplified D1/D2 domain from G. fermentans and lane 3, negative control.

Amplification of the genomic DNA yielded 600bp fragment which correlated with the expected 600bp D1/D2 domain in ascomycetous yeasts. To verify that the PCR product was the divergent D1/D2 domain from *G. fermentans,* the PCR product was sequenced from both ends. Two sequences were obtained and assembled. A 99 % sequence identity with 26S rDNA gene of *G. fermentans* at nucleotide level obtained indicated that the amplified PCR product was a 26S rDNA. of *G. fermentans* (Accession U40117), from the 545 compared nucleotide, 541 were identical and the remaining four exhibited Single nucleotide polymorphism (Figure 3.14). Thus, confirming the identity of the yeast to be *G. fermentans*. In multiple alignments, the yeast strain under-study is referred to as sample.

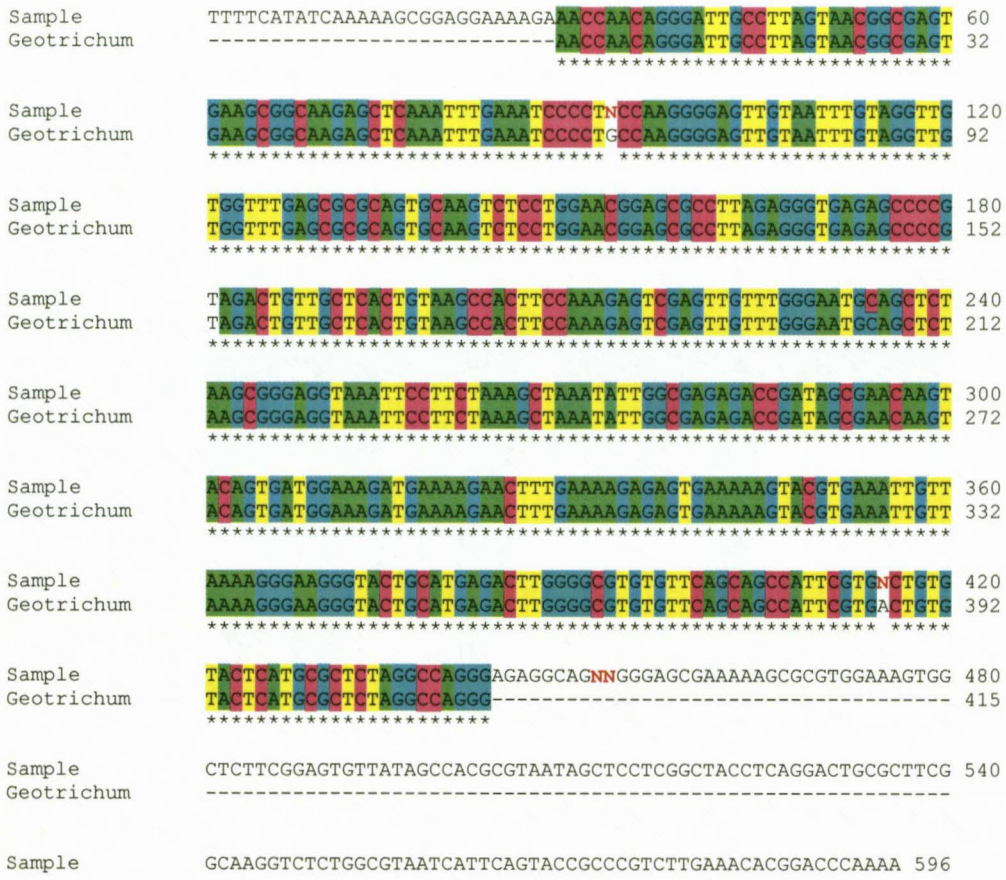

Figure 3.14: Multiple alignment of the sequenced D1/D2 domain and *G. fermentans* (ACCESSION U40117).

3.4 Conclusions

The proteins responsible for gold nanoparticle formation could be successfully partially purified and specific activity enhanced 15 times using two anion exchange columns.

Gold nanoparticle formation ability was lost with more purification steps. The activity could be slightly enhance by the addition of NADH, yet the protein displayed no iron reductase activity but rather correlated to literature's suggestion that this protein could also have nitrate reductase activity. This suggests a nitrate reductase to be responsible for gold nanoparticle formation or that a protein that is able to accept both nitrate and gold into the active centre and catalyse the nanoparticle formation.

In characterization of the nanoparticle formation we have established that physico-chemical factors can influence nanoparticle formation. Where TEM analysis revealed the average size of the formed particles to be 15 nm, and the nanoparticles were confirmed by EDS to be elemental gold. The formed gold nanoparticles were polycrystalline in nature.

Even though nitrate reductase normally catalyzes the reduction of nitrate which is an anion, it was also able to reduce a cation in a form of gold(III). The phenomenon of one enzyme catalyzing several reactions is known for many enzymes, especially nitrate reductases given the scope of their partial activities.

3.5 References

Ahmand, A., Senapati, S., Khan, I. M., Kumar, R. and Sastry, M. 2005. Extra/intracellular biosynthesis of gold nanoparticles by an alkalotolerant fungus, *Trichothecium* sp. *Journal of Biomedical Nanotechnology.*, ***1:*** 47 – 53

Anil, K, Abyaneh, MK, Gosavi, S.W, Kulkarni, S.K, Pasricha R, Ahmad A and Khan, M.I. 2007. Nitrate reductase-mediated synthesis of silver nanoparticles from $AgNO_3$. *Biotechnology Letters.*, **3:** 439 – 445

Aslan, K., Lakowicz, J.R. and Geddes, C.D. 2005. Nanogold plasmon resonance-based glucose sensing. 2. Wavelength-ratiometric resonance. *Analytical Chemistry.*, **77:** 2007 – 2014

Barbier, G.G and Campbell, W.H. 2005. Viscosity of eukaryotic nitrate reductase activity. *Journal of Biological Chemistry.*, **280:** 26049 – 26054

Bester, A.P. 2007. Iron reductase activities of *Thermus scotoductus*-assigning functionality to the soluble protein.,Thesis (unpublished)

Carrot, G., Valmalette, J. C., Plummer, C. J. G., Scholz, S. M., Dutta, J., Hofmann H. and Hilborn, J.G. 1998. Gold nanoparticle synthesis in graft copolymer micelles. *Colloid and Polymer Science.*, **276:** 853 – 859

Chah, S, Fendler, J. H. and Yi, J. 2002. Nanostructured gold hollow microspheres prepared on dissolvable ceramic hollow sphere templates. *Journal of Colloid and Interface Science.*, **250:** 142 – 148

Durán, N., Marcato, P., Alves, O., de Souza, G. and Esposito, E. 2005. Mechanistic aspects of biosynthesis of silver nanoparticles by several *Fusarium oxysporum* strains. *Journal of Nanobiotechnology.*, **3:** 1 – 7

Eckardt, N.A. 2005. Moco Mojo: Crystal structure reveals essential features of eukaryotic assimilatory nitrate reduction. *The Plant Cell.*, **17:** 1029 – 1031

Eustis, S and El-Sayed, M.A. 2005. Why gold nanoparticles are more precious than pretty gold: Nobel metal surface plasmon resonanceand its enhancement of radiative and nonradiative properties of nanocrstals of different shapes. *Chemial Society Reviews.*, **35:** 209 – 217.

Feinberg, F. and Holden, F. 2006. Charaterization of Dissimilatory Fe(III) versus NO_3^- reduction in Hyperthermophillic Archaeon *Pyrobaculum aerophilum. Journal of Bacteriology.*, **188:** 525 – 531

He, S., Guo, Z., Zhang, Y., Wang, J. and Gu, N. 2007. Biosynthesis of gold nanoparticles using the bacteria *Rhodopseudomonas* capsulate. *Material Letters.*, **61:** 3984 – 3987

Kurtzman, C.P. and Robnett, C.J. 1998. Identification and phylogeny of ascomycetous yeasts from analysis of nuclear large subunit (26S) ribosomal DNA partial sequences. *Antonie van Leeuwenhoek.*, **73:** 331 – 371

Labuschagne, M. and Albertyn, J. 2007. Cloning of an epoxide hydrolase-encoding gene from *Rhodotorula mucilaginosa* and functional expression in *Yarrowia lipolytica.*, **24:** 69 – 78

Meldrum, F.C, Wade, V.J, Nimmo, D.L, Heywood, B.R. and Mann, S. 1991. Synthesis of inorganic nanophase materials in supramolecular protein cages. *Nature.*, **349:** 684 – 687

Meyer, S.A., Payne, R.W. and Yarrow, D. 1998. *Candida* Berkhout. pp, 454 – 573. In: Kurtzman, C.P. and Fell, J.W. (eds). The yeasts, a taxonomic study. Elsiver, New York, USA

Mitt, R., Grant, B, and Heideman, W. 1990. Adenylate cyclase in *Saccharomyces cerevisiae* is a peripheral membrane protein. *Molecular and Cellular Biology.*, **10:** 3873 – 3883

Niemeyer, C.M. 2001. Nanoparticles, proteins and nucleic acids: Biotechnology meets materials science. *Angewandte Chemie International Edition.*, **40:** 4128 – 4158

O'Donnell K . 1993. *Fusarium* and its near relatives. pp, 225 – 233. In: Reynolds DR & Taylor JW (Eds). The fungal holomorph: Mitotic, meiotic and pleomorphic speciation in fungal systematics. CAB International, Wallingford, UK

Opperman, D.J. and Heerden, E. 2008. A membrane-associated protein with Cr(VI)-reducing activity from *Thermus scotoductus* SA-01. *Federation of European Microbiological Societies Microbiology Reviews.*, ***280:*** *210* – 218

Sear, R.P. 2007. Nucleation: theory and applications to protein solutions and colloidal suspensions. *Journal of Physics: Condensed Matter.*, **19:** 1 – 28

Shivshankar, S, Rai, A, Ahmad, A. and Sastry, M. 2004. Rapid synthesis of Au, Ag and bimetallic Au core-Ag shell nanoparticles using Neem (*Azadirachta indica*) leaf broth. *Journal of Colloid Interface Science.*, **275:** 496 – 502

Showe, K. and DeMoss, A. 1968. Localization and regulation of synthesis of nitrate reductase in *Escherichia coli. Journal of Bacteriology.*, **95:** 1305 – 1313

Smith, P.K., Krohn, R.I., Hermanson, G.T., Mallia, A.K, Gartner, F.H., Provenzano, M.D., Fujimoto, E.K., Olson, B.J. and Klenk, D.C. (1985). Measurement of protein using bicinchoninic acid. *Analytical. Biochemistry.*, **150:** 76 – 85

Stookey LL. 1970. Ferrozine a new spectrophotometric reagent for iron. *Analytical Chemistry.*, **42:** 779 – 781

Yoshimura, H. 2006. Protein assisted nanoparticle synthesis. *Colloids and Surfaces A.*, **282-283:** 464 – 470

Chapter 5

Summary

Biological systems are used to build nanoparticles of specific morphology and function (Eustis and El-Sayed, 2005). The difficulty in synthesizing nanoparticles of the desired size, shape and monodispersity directs research into new and redefined synthetic methods. The microbial interaction with metals might also supply eco-friendly methods for metal nanoparticle production. Various yeast species obtained from UNESCO MIRCEN Yeast culture collection at UFS were evaluated for their ability to reduce Au^{3+} ions into elemental gold nanoparticles by visual analysis. Colour intensity and time taken for the biomass to turn purple were used to select for those organisms which are able to reduce gold. The ability of whole cells to reduce Au3+ ions was dependent on concentration of gold(III) ions and (contact) time. Transmission electron microscopy (TEM) micrographs of *Candida viswanathii, Geotrichum fermentans* and *Rodotorula graminis* showed cell bound nanoparticles. Cell free extracts of the above mentioned three species showed enhanced gold reduction over a shorter period. Physicochemical parameters such as pH, gold concentration and temperature influenced the reduction and particle formation. From sub-cellular fractionation, the cytoplasm showed higher gold reduction activity. Partial purification was achieved in two anion exchange chromatography steps and 15 fold nanoparticle gold reduction activity as well as 20 fold nitrate reductase activity. The partially purified fraction exhibited both nanoparticle formation and nitrate reductase activity. The nanoparticles formed were confirmed to be gold by EDS analysis and electron diffraction patterns were characteristic of polycrystalline material. The average size of the formed gold nanoparticles was 15 nm.

Keywords: ions, G. fermentans, gold, nanoparticles, reductase

Chapter 6

Opsomming

Biologiese sisteme word gebruik om nanopartikels te bou met spesifieke morfologie en funksie. Die moeilikheidsgraad in die sintese van nanopartikels met die verlangde grootte, vorm en monodispersiteit rig navorsing na nuwe en hergedefinieerde sintetiese metodes. Die mikrobiese interaksie met metale mag ook eko-vriendelike metodes verskaf vir metaal nanopartikel produksie. Verskeie gisspesies verkry vanaf *UNESCO MIRCEN* Giskultuurversameling by UVS is geëvalueer vir hul vermoë om Au^{3+} ione te reduseer na elementêre goud nanopartikels deur visuele analise. Kleurintensiteit en tydsverloop totdat die biomassa na pers verkleur het, is gebruik om te selekteer vir organismes wat goud kon reduseer. Die vermoë van heel selle om Au^{3+} ione te reduseer was afhanklik van die konsentrasie van die Au^{3+} ione en kontak tyd. Transmissie eletron mikroskopie (TEM) mikrograwe van *Candida viswanathii*, *Geotrichum fermentans* en *Rodutorula graminis* het assosiasie van nanopartikels met die sitoplasma getoon en sommige was seloppervlak-gebonde. Dit mag 'n aanduiding wees dat elke organisme 'n unieke, eiesoortige meganisme het om oormatige goud in sy eie omgewing te verwerk. Sel-vrye ekstrakte van bogenoemde drie spesies het verhoogde goudreduksie getoon in 'n korter tydsperiode met hoër konsentrasies goud. Fisiochemiese parameters soos pH, goudkonsentrasie en temperatuur het reduksie en partikelvorming beïnvloed. Vanaf sub-sellulêre fraksionering het die sitoplasma hoër goudreduksie aktiwiteit getoon. *G. fermentans* is gekies vir finale karakterisering van die nanopartikel meganismes gebruik deum hierdie gisspesie.Gedeeltelike suiwering van die proteïen/ensiem betrokke in nanopartikel-vorming is gedoen in twee anioon-uitruilingskromatografie stappe. 'n 15-voud nanopartikel goudreduksie aktiwiteit asook 'n 20-voud nitraat reduktase aktiwiteit is getoon met die finale proteïenfraksie. Die gevormde nanopartikels is bevestig as suiwer goud deur (Energie dispersiewe X-straal spektroskopie) EDS analise en die elektron diffraksiepatrone was kenmerkend van polikristallyne materiaal. Die gemiddelde grootte van die gevormde goud nanopartikels was 15nm.

Sleutelwoorde: G. fermentans, goud, nanopartikels, biologiese reduksie, nitraat reduktase